UNIVERSIDADE
BEIRA INTERIOR

SATELLITE FORMATION FLYING CONTROL OF THE RELATIVE TRAJECTORY SHAPE AND SIZE USING LORENTZ FORCES

Gonçalo da Costa Amaro

Dissertação para obtenção do Grau de Mestre em
Engenharia Aeronáutica
(Mestrado integrado)

Orientador: Prof. Dra. Anna Guerman
Orientador: Dr. Danil Ivanov

Outubro de 2021

Acknowledgements

There are many people to whom I would like to acknowledge my deepest gratitude for helping me over this long path.

Firstly, I would like to thank professor Anna Guerman for introducing me to this theme and to whose I am grateful to have worked with.

My deepest gratitude goes also to Dr. Danil Ivanov, my tireless mentor throughout the development of this work whose patience, dedication, and perseverance were truly admirable. I rejoice in all the criticism and wisdom shared that genuinely made me grow either as a person and as the professional that I am about to become.

To my family for their immense love, encouragement, and understanding, my eternal gratitude. Especially to my parents, Sandra and José, for providing me the opportunity to follow this academic path but also for the endless love and trustfulness. To you, I am eternally grateful.

At last, I would like to thank all of my friends who supported and shared with me both the best and the worst moments during this journey.

Resumo

Métodos de controlo para formações de voo de satélites de pequenas dimensões que não recorram ao uso de combustível representam, atualmente, um interesse especial e uma importante vantagem para a indústria espacial. Nesta dissertação é proposto um algoritmo de controlo que, recorrendo à força de Lorentz em orbitas terrestres baixas (LEO), é capaz de alcançar trajetórias com o respetivo o formato e o tamanho desejados. A força de Lorentz resulta de uma interação entre o campo magnético terrestre e o satélite eletricamente carregado. Alcançar as trajetórias solicitadas revela-se como sendo um desafio visto que o único método de controlo é a variação da carga interna do satélite. Este mecanismo de controlo revela-se como sendo incapaz de conferir controlabilidade total ao dispositivo. Um controlo baseado no método de Lyapunov é desenvolvido com o objetivo de eliminar a deriva inicial do satélite após o lançamento orbital e é destinado a atingir o tamanho e formato predefinidos da trajetória relativa objetivo. O algoritmo de controlo é construído de forma a corrigir os diferentes parâmetros da trajetória relativa em diferentes posições relativas. Usando a força de Lorentz é possível atingir tanto as amplitudes objetivo, considerando ambos os movimentos dentro e for do plano da trajetória, mas também a deriva e o deslocamento relativos da trajetória. Devido à falta de controlabilidade total, o algoritmo desenvolvido é incapaz de corrigir completamente os movimentos dentro e fora do plano da trajetória, visto que estes parâmetros são definidos na sua totalidade pelas condições de lançamento e, como tal, arbitrários. O algoritmo de controlo proposto possibilita a convergência dos valores para o formato e tamanho da trajetória desejada.

Ambas as estratégias de controlo centralizadas e descentralizadas são aplicadas e a respetiva performance estudadas. No caso da estratégia centralizada, é considerado um voo em formação composto por dois satélites, onde o Líder se revela como sendo eletricamente neutro enquanto, e prescrevendo uma trajetória terrestre baixa circular, enquanto que o segundo, eletricamente ativo, é capaz de alterar o seu posicionamento relativo requerido, permutando a sua carga interna. Uma formação de voo considerando um número superior a dois satélites, com capacidades de carregamento elétrico, é também controlável considerando o algoritmo proposto. Este trabalho tem também em consideração o controlo da trajetória de um swarm de satélites num formato esférico. Simulações numéricas são usadas como método de análise da performance do algoritmo desenvolvido. Durante o processo de análise é implementado o modelo do dipolo inclinado como forma de simular o campo magnético terrestre. É também aplicado um algoritmo responsável por evitar situações de colisão eminente para casos em que a convergência de movimento dos satélites entra em zonas de proximidade critica. O tempo de convergência e a precisão da trajetória final são avaliadas para diferentes parâmetros e condições de simulação.

Palavras-chave

Formação de voo; Mecânica orbital; Algoritmo de Controlo; Algoritmos de controlo baseados na função de Lyapunov; Matlab; Lorentz force.

Abstract

Propellantless control approaches for small satellite formation flying represent a special interest and an important advantage for space industry nowadays. A formation flying control algorithm using the Lorentz force for Low-Earth Orbits to achieve a trajectory with required shape and size is proposed in this dissertation. The Lorentz force is produced as the result of interaction between the Earth's magnetic field and an electrically charged spacecraft. Achieving the required trajectories represents a challenge since the control is the variation of the satellite's charge value. This control mechanism simplicity cannot provide full controllability. A Lyapunov-based control is developed for elimination of the initial relative drift after launch and it is aimed for reaching a required relative trajectory with predefined shape and size. The control algorithm is constructed to correct different parameters of the relative trajectory at different relative positions. The required amplitudes for close relative trajectories for in-plane and out-of-plane motion as well as the relative drift and shift of elliptical relative orbits are controllable using Lorentz force. Due to the absence of full controllability, the algorithm is incapable to correct the in-plane and out-of-plane motion phases, once these parameters are defined by the deployment conditions and therefore arbitrary. The proposed control allows the convergence to the trajectory with required shape and size.

Centralized and decentralized control approaches are implemented and their performance is studied. The centralized approach considers two satellites formation formed by an electrically neutral leader satellite moving on a circular LEO and a follower which actively controls its orbital motion by changing its charge in order to remain in close vicinity of the leader. Formation flying consisting of more than two satellites with charge-changing capability can also be controlled by the proposed algorithm using a decentralized approach. This work also considers the control of satellite swarm trajectories in a sphere-shaped formation. Numerical simulation of the relative motion is used to study performance of the control algorithm. It implements the model of the geomagnetic field as a tilted dipole. The repulsive collision avoidance control is proposed for the case when the system elements are inside a dangerous proximity area. The convergence time and final trajectory accuracy are evaluated for different simulation parameters and conditions.

Keywords

Formation Flying; Orbital mechanics; Control algorithms; Lyapunov-based Control algorithms; Matlab; Lorentz force.

Contents

List of Figures

List of Tables

List of Acronyms

CEP	Celestial Ephemeris Pole
COTS	Comercial Off The Shelf
ECI	Earth-Centered-Inertial
ECEF	Earth-centered Earth-fixed
EMFF	Electromagnetic Formation Flying
ESA	European Space Agency
FF	Formation Flying
FRF	Form Factor
GOSTM	Upper Atmosphere Model for Ballistic Calculations
GPS	Global Positioning System
HCW	Hill-Clohessy-Wiltshire
IGRF	International Geomagnetic Reference Field
LAO	Lorentz-Augmented Orbits
LEO	Low-Earth Orbits
LF	Leader/follower
LVLH	Local-Horizontal Local-Vertical
MIMO	Multiple-Input-Multiple-Output
NASA	National Aeronautics and Space Administration
OE	Orbital Elements
RAAN	Right Ascension of the Ascending Node
TPF	Terrestrial Planet Finder
U	CubeSat unit
UBI	Universidade da Beira Interior
VS	Virtual Structure

Nomenclature

Greek symbols

β Magnetic current rotation relative to the Greenwich's longitude

β_{G0} Greenwich's longitude

δ Argument of Perigee

δ_{J_2} Body's J_2 effects on the absolute position vector

γ Angle measured between the Magnetic pole and the Geocentric north pole

μ Gravitational parameter

Ω Right Ascension of the Ascending Node

ω_e Earth's angular rotation rate

ϕ Orbital angular velocity in Hill's frame

τ Time since perigee passage

θ True anomaly

$\tilde{\omega}$ Dipole's angular rotation

υ_n Normal velocity

υ_r Radial velocity

Other variables and constants

$\ddot{\mathbf{r}}$ Relative acceleration vector

$\ddot{\mathbf{R}}_1$ Absolute acceleration of body 1

$\ddot{\mathbf{R}}_2$ Absolute acceleration of body 2

$\hat{\mathbf{N}}$ Earth dipole direction unit vector

$\hat{\mathbf{u}}$ Unit vector pointing from body 1 into body 2

$\hat{x}, \hat{y}, \hat{z}$ ECEF's frame axis

$\mathbf{a}_{J_2}$ Body's J_2 acceleration effects

$\mathbf{B}$ Earth's magnetic field model

$\mathbf{E}$ Earth's electric field model

$\mathbf{F}_{12}$ Body 1 resultant gravitational attraction acting on body 2

$\mathbf{F}_{21}$ Body 2 resultant gravitational attraction acting on body 1

$\mathbf{L}_F$ Lorentz force vector

$\mathbf{r}$ Vector directed from body 1 into body 2

$\mathbf{R}_o$ Initial position

$\mathbf{R}_1$ Body 1 position vector

$\mathbf{R}_2$ Body 2 position vector

$\mathbf{r}_{ab}$ Relative position vector in Hill's frame

$\mathbf{R}_i$ Body's position vector in the ECI frame

$\mathbf{R}_S$ Satellite's position unit vector

$\mathbf{r}_S$ Satellite's position unit vector's magnitude

$\mathbf{V}_o$ Initial velocity

$\mathbf{v}_{ab}$ Relative velocity vector in Hill's frame

$\mathbf{V}_i$ Body's velocity vector in the ECI frame

$\mathbf{x}_{ab}$ Equation of the relative motion in Hill's frame

$\mathbf{X}_i$ Body's state vector in the ECI frame

A Hill's frame transformation matrix

a semimajor axis

A_1 First Euler angle transformation cosine matrix

A_2 Second Euler angle transformation cosine matrix

A_3 Third Euler angle transformation cosine matrix

b semiminor axis

B_0 Earth's magnetic dipole moment

E Eccentricity anomaly

e Eccentricity

G Universal gravitational constant

h Body's relative angular momentum per mass unit

i Inclination

J_2 Coefficient for Earth's second harmonic

M Orbital mean anomaly

m_1 Body's 1 mass

m_2 Body's 2 mass

p Semi-latus rectum

q Body's charge value

r Vector R magnitude

r_c Bodies 1 and 2 center of mass

t Current time

t_p Passage time at the periapsis

x', y', z' Hill rotating frame conversion operators

X, Y, Z ECI's frame axis

x, y, z Hill's frame axis

Chapter 1

Introduction

1.1 Personal Motivation

The current days demand a renewed vision on the overall technology used in several distinct areas, from the daily transportation means to the state of art technologies used in the science of outer space exploration. This is a fact, not only motivated by the rising ecological awareness but also because of its economical interests involved in the recent engagement of private companies in the modern-days ”Space 2.0”[1].

Two of the most interesting promising subjects, appealing to both ecological and economical branches, are satellite miniaturization and the adoption of alternative means of systems for motion control opposite to the classical onboard propulsion systems. In the light of these scientific and exploring necessities, this thesis endorses exactly these two subjects, providing a study on the possibility of using a propellantless motion control system in order to maintain a satellite flying formation.

To achieve such results, this work focuses on the utilization of the Lorentz electromagnetic force to actively control the translational motion of each satellite to keep a formation configuration. The possible outcomes of this type of motion control could mean a new option, with not only ecological (once it means a renewable and ”green” magnetic interaction) as well as more room for onboard equipment once the propellant tanks and systems are no longer needed.

In the light of this, the author of this M.Sc. thesis aims to not only present a valid and rigorous study of relative motion control using a revolutionary LAO(Lorentz-Augmented Orbits) technology in the small satellites field, but also to take a small step towards innovation in this technological field, hoping to inspire some minds into looking on the development and study of such alternative systems and into a new chapter of space exploration.

The results obtained from this work have been published in the conference paper , indexed in Scopus [2].

1.2 Purposes and Objectives of the Project

This master thesis is presented as an investigation path in the development of renewable formation control systems that will prospectively replace the classic fuel based ones. This

project aims to advance the research of the possible usage of the interaction between the spacecrafts and the orbital environment as means of propellantless relative position control systems.

The developed work in this master thesis has the ultimate goal of validating the usage of the electromagnetic Lorentz force for the elimination of the relative drift in formation flying configurations composed by two or more satellites. Therefore, through the development of the control algorithm and along the simulations, the results prove that not only this relative drift could be controlled and eliminated, but also revealed that it could be used in a more ambitious way. Thus, the following objectives were defined:

- Examine the nature of the Formation Flying missions and investigate the necessary steps that are necessary to develop a fully autonomous control algorithm and system.
- Examine the Lorentz force scientific theme through extensive literature review and formulate the scientific case for the possible usage of this effect as a control method.
- Identify the simulation needed and propose the different mission scenarios to be tested in order to offer an extensive scope of results.
- Develop a set of different formation configurations to test the developed control algorithms in the system's performance.
- Examine the impact of different environmental effects on the formation configuration maintenance and its influence in the relativemoi+tion control of Lorentz capable devices.
- Propose a possible draft for a Lorentz force device controlling algorithm.
- Propose future work to be developed and the further steps of investigation.

1.3 Thesis Outline

This thesis subject is presented in a coherent and logical manner. The description of each chapter within this document is presented as follows:

- In Chapter 1 an introduction is given clarifying the author's motivation to investigate the possible usage of Lorentz capable systems for the relative orbital positioning in Formation Flying configurations. It also presents an overall view on the expected research results and the possible contributions of the investigation to the scientific community.
- The Chapter 2 gives a theoretical introductory insight on the themes addressed in the current work, presenting a special insight in the CubeSat technology and enhances its

major role in numerous fields. Furthermore, this chapter also provides an overview on the scientific theme as well as a review of the state-of-art former researches both in Formation Flying field and in Lorentz control field.

- The Chapter 3 provides a general overview on the orbital dynamics in the LEO environment as well as the main environmental effects influencing the motion of the satellites in the formation.

- In Chapter 4, the development steps of the control algorithm are clarified. Here, firstly is present the base theory functions, later adapted to the control studied in the current work. Afterwards, a detailed explanation of the development stages of the control algorithm is presented, finishing with an explanation of the slight adaptations on the general algorithm accordingly to the different simulation scenarios.

- In Chapter 5 the simulation results are presented for the different formation scenarios examined. Along with the numerical results, are presented the graphics depicting the obtained trajectories during the Monte Carlo simulations.

- Chapter 6 presents the conclusions on the results of the study and proposes the future adaptations and investigations that can be preformed in order to make this technology possible.

Chapter 2

Literature Review

Technology development is profoundly connected with the society's evolution, a connection witnessed from the earliest beginnings to the present days, in such a way that our modern lives would reveal to be impossible without this linkage. Global Positioning Systems (GPS), weather forecasting, mobile networks, television services or national security are just a few of the most easily noticeable applications related to space exploration, specifically when considering the advances registered in satellites field for the last few decades [3][4].

The satellite miniaturization witnessed in the space industry is a developing trend since these small-sized types of equipment offer a new sort of advantages mainly related to the manufacturing time and representing a simplification when concerning the launch opportunities [5]. However, these size miniaturization trend comes with a compromise respecting the limitation of the on-board power capabilities due to the size restrictions, a characteristic that also contributes to their short lifetime and a more action limited motion control system. Nevertheless, all of these disadvantages are easily overcome when considering the dynamic performance of missions concerning the usage of multiple spacecraft systems. Therefore, emerging technology such as satellite formation flying configurations reveals a major interest to the scientific community, where a group of small satellites can substitute larger ones in key missions and even solve near-Earth issues that cannot be handled by single larger satellites [6].

Another associated advantage is the facilitated usage of external disturbance forces to control the relative motion of the satellite. Besides the fact that alike propellantless systems can be applied on all types of satellites, the smaller dimensions of devices such as CubeSats enables the easier implementation of such systems. These control approaches perspectives have been widely studied over the last two decades, and will be discussed and analyzed further in this chapter.

This chapter's objective is to give an insight into the works done in the small satellite formation flying field and the respective control approaches, serving as a knowledge basis for the development of this thesis. Firstly, an introductory section is presented giving a general description and evolution of the satellites technology from its beginnings to the expected breakthrough technology to be presented in the near future time. The next section focuses on the formation flying concept, where it is introduced and presented. It is then followed with an insight on the Lorentz force technology and the latest achievements. To finalize, an insight on the Lorentz force technology is given.

2.1 The rise of small satellites

The successful radio response received from the orbiting Sputnik-1, dated in the year of 1957, marked the birth of the space exploration age. Sputnik-1 was therefore the first artificial satellite to be intentionally placed in orbit. From this year, the space technology conquered a place in the technological development industry and it is nowadays a needed asset for the daily activities that we consider to be as essential [7].

As any other technological system, satellites are only a piece of the overall components that together make the mission accomplishment possible. Usually, a space mission can be divided into three main segments: the ground segment, responsible for the communication and representing the mission ”brain”; the launch segment, which is responsible for the transportation into orbit; and finally the space segment, where the satellites are the main actuators, which perform the mission objectives [3] [8].

A satellite’s design is highly dependent on the functions it is developed to perform, therefore there is a large variety of satellite types and dimensions, that results in a classification that sorts these systems either by mission or by mass. Mission classification stands for the general purposes that fostered the satellite design in order to accomplish the functions required by the user’s needs [1][8][7].

As for mass classification, the different masses sorting is presented in the table 2.1

Class	Mass Range (kg)
Conventional large satellites	> 1000
Conventional small satellites	< 1000
Minisatellite	< 500
Microsatellite	< 100
Nanosatellite	< 10
Picosatellite	< 1
Femtosatellite	< 0.1

Table 2.1: Classification of the satellites accordingly to their total mass.

However, satellite dimensional evolution has suffered significant changes throughout space exploration history, with several influencing factors taking a toll in this ”size” evolution. The recently witnessed dimensional shortening trend was mainly influenced by increasing space accessibility and a growing industry competitiveness in the last two decades.

The total mass of these equipment’s grew as science and the space race demanded increasingly more intricate and complex devices. The available launchers capabilities and the finance and technological infrastructures were the main limiting factors for this dimensional growing trend, as space-faring nations required a highly developed technological base with huge investment. This resulted in the restrictive space exploration — an exclusive ”club” of

space ”haves” with enormous military, economic and cultural advantages over space ”have-nots”[1].

Changing world politics and military emphasis in the last twenty years has brought about a quiet revolution in space. This exploration revolution brought to an end the long sovereignty witnessed since the cold war, where the large and complex spacecrafts were only accessible by giant corporations such as NASA, Roscosmos or ESA, with government-backed funds. New concepts and ideas were often hold back due to the significant risk of failure, which by its hand would mean the lost of millions and could negatively influence future investments.

However, the need for development and the lack of open positions for people with little experience in what concerns space mission designs originated the birth of the so called new space program. This was a huge step in the modern exploration phase that hatched an entirely new economy market, opened for all those who are keen to start with an open mind and incorporate innovative ideas into designs without the corporations fear of failure [3]. Furthermore, there was the need to resort to the current advances in microelectronics, software, and material science in order to create lower-cost and more responsive systems. Resuming, the fast paced space industry took its first steps just a couple of decades ago, born from an ideological fusion between the technological modernization need, with the determination and willingness of a generation to face and accept the risks inherent to innovation.

With this revolution a new era in small satellites began, with the rise of the Cubesat and the small satellites advent. The CubeSat is a standardized subclass of the small satellites and it was developed in a cooperation between Stanford and California Polytechnic State University during the year of 1999, with the scholar objective of involving students in the space industry and giving them some major engineering skills concerning the mission design and management at the same time [1]. The CubeSat term come after the Form Factor of 1U unit, i.e., one unit represents a 10-centimeter cube ($10 \times 10 \times 10\ cm^3$) with a total mass of up to 1.33 kg (Figure 2.1).

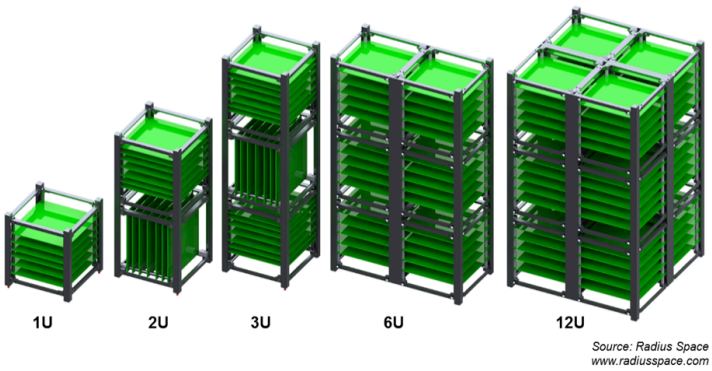

Figure 2.1: CubeSat modules configuration. (Credit from [9])

This configuration characteristic permits the 1U unit to serve not only as a stand alone satellite, but also the possibility to be combined, together with other units, into a larger spacecraft in case of a mission that requires a larger amount of on-board capacity.

The standardization feature of these systems promotes a highly adaptive, highly reliable system where satellite components are available for an affordable price, with a market, "Commercial Off The Shelf" (COTS), offering a large variety products from several different suppliers that can be combined according to the needs of the mission [1][3]. In addition, the dimensional aspect of these systems enables the simplification of the launching process, since the units can be released in orbit as secondary payloads (piggybacks). CubeSat-like technology enables a wider launching window, decreasing both launch and development costs. Adding the fact that having a less complex configuration the preparation process is faster than the more traditional spacecrafts representing a low-cost solution that turns the space accessible for almost everyone. This accelerated schedule allows students from universities with a CubeSat program to be involved in the complete life cycle of a mission [1].

Developed initially as educational tools, CubeSat technology is now gaining a wider role in scientific community and in the commercial space industry, where this small satellites are starting to prove their value after their enormous potential in terms of high-quality scientific research and economic revenue [1][4]. The last ten years are a perfect example of the significant slice that this technology is taking in the industry and the future perspectives are to persevere this growing tendency (Figure 2.2).

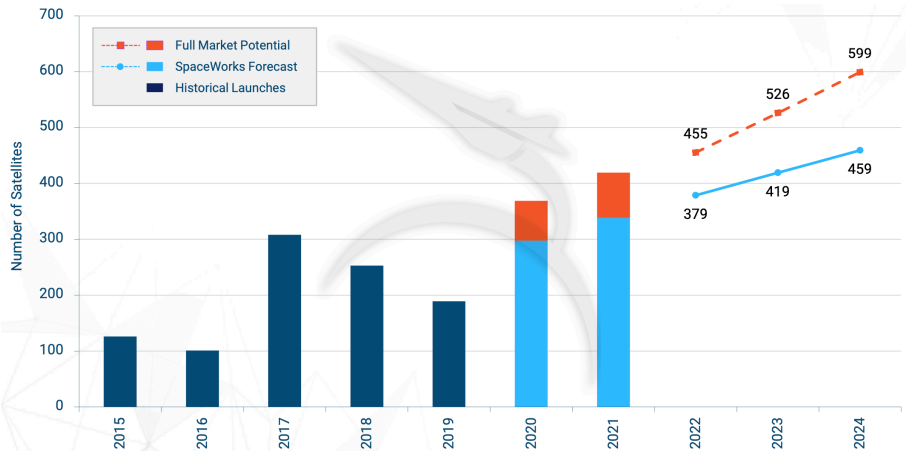

Figure 2.2: Nano/Microsatellite lauching history and forecast since 2015(Credit from [4]).

As the Figure(2.2) depicts, CubeSat technology is a growing market in the space exploration field, that will certainly play a vital role in future space activities. Capable of providing space access to smaller nations, to educational institutions, or even for commercial organizations, enabling the development and launch of low-cost spacecraft for institutions with limited budgets. Along with these, it is even possible to acquire affordable and ready-to-use COTS components, simplifying the satellite development process [3]. The added capacity of en-

abling the construction/implementation of large constellations of small-sized satellites, with performances similar or even greater compared to traditional-sized satellites, contributes to growing investment in this technology worldwide[10].

2.2 Review on Formation flying and its advantages

A satellite formation flying is defined as a set of satellites moving in close relative trajectories that can control their relative position and/or relative velocities, keeping close distances and solving a common problem[11].

Recently, a lot of attention has been given to formation flying missions, as the recognition for the benefits of using satellite clusters grows and more research is carried out in the area. The concept of formation flying holds a new range of possibilities that can be looked upon as an alternative to the traditional concepts available, such as the replacement of large satellites by several smaller ones flying in a designed controlled formation [12]. The transition from single satellite paradigms to the multiple elements operation could signify a tremendous improvement either in the global time development or in the overall cost of the system. Additionally, the formation flying concept offers mission flexibility and robustness that no monolithic satellite mission can, once the total failure of one of the elements does not results in the total failure of the mission [13]. The possibility of augmenting, expanding, or even reconfiguring the formation are also looked upon as extra advantages for this mission concept, making it possible to add new applications and innovate the mission's primary purpose.

Lastly, the spatially distributed placement of the elements inside the configuration allows the gathering of more accurate scientific data. Future planned missions aim to push further the boundary of what can be achieved by the formation flying technology [14], [15]. However, the formation flying concept is conjugated with challenging questions concerning the autonomous ability to control the relative motion with or without limited ground guidance [16]. Historically, the first projects using the formation flying concept, aiming for automatic rendezvous situations or even docking control between two distinct spacecraft, were developed for the Apollo missions, and later used in other major projects such as the Space shuttle, Skylab, or Gemini missions [13].

A spacecraft formation can be considered as a distributed system. The relative motion control systems of the individual spacecraft act as the local control agents. The control decisions of the local control agents must be coordinated to ensure the stability and convergence of the global system [13]. Typically, in the formation flying field, it is possible to divide these control strategies into two opposite fields: centralized and decentralized controllers, a distinction that is defined based on where and who makes the control decisions[16].

The definition of a centralized system describes a formation where the system configuration is controlled by a single control agent, often named as mother, i.e., this strategy accounts with a single spacecraft responsible for continuously monitor the other system elements rel-

ative state. TechSat 21 is the perfect example of this type of controlling strategy [17]. This was mission which was designed with the purpose of testing but also validate the on-going technology improvements and the preliminary findings on the formation flying field. The mission examines the overcoming challenges needed to face when proximity operations are required. This mission took place between late 2003 and mid 2004, in which the performance of a Leader/Follower approach with a centralized strategy was evaluated. The control was aimed to maintain the required configuration in a near circular orbit at a $500-550$km altitude. During this mission one year lifetime, and apart from demonstrating the capabilities of formation flying (achieving the required precision of a millimeter level), this study also enabled the development of several control approaches for fuel minimization. Another case of a centralized architecture for FF is [18], where a renewed control technique which reveals to be able to control the rotation of the entire system about a predetermined axis is presented. The proposed controller can individually synchronize both the translational motion and the attitude motion of the individual satellites in the formation, however both environmental and implementation disturbances were not considered during the simulations. Pan and Kapila et al. also propose a controller for coupled translational and attitude dynamics using the centralized approach. The authors in the study [19] present a nonlinear controller derived from a Lyapunov framework that is capable of correcting the follower's expected relative translational and relative attitude motion.

Opposite to this, in decentralized systems, control decisions are delegated to the local control agents. Therefore, every single unit is capable to control its relative motion based on the information obtained either by the communication between the neighboring peers or from local observations. This robustness characteristic represents an advantage considering that it implies fewer risks for the mission along with the relatively simple control laws [13]. In a centralized approach, a critical failure in the mother element would imply the formation compromise and the consequent loss, while the architecture of a decentralized system permits the failure of single elements of the formation [16], [11]. Since this failure reveals to be confined locally in the region of the failed control agent, it results in a graceful degradation of the system's performance[13]. Also, this kind of system control strategy enables the simplification of the used control laws because the global controller design can be divided in several smaller control agents [20], [16].

Besides formation controlling strategies, it is also important to define the control approaches that will define the general configuration for the satellite's formation flying. Bearing in mind the mission objectives different control schemes can be applied to formation flying missions. The most commonly used schemes for motion control are listed and clarified as follows [11], [16]:

- Orbit Tracking: normally used for single satellite missions, is a simple approach that focuses on the occupation of a specific orbit using recurrent station-keeping maintenance maneuvers. Additionally, this technique may be used in the establishment of formation flying, with the beneficial characteristic of presenting a control method that

requires little, in some cases null, cooperation or coordination between the satellites in the system. However, and despite the satellite autonomy being an advantage, this scheme entails the need for more maneuvers to achieve the desired configuration when in comparison to other control models that rely on the synchronous action of the satellites in the formation. The TanDEM-X mission is presented as one of the best examples of this type of configuration, Fig. 2.3 [21]. The mission was designed to generate a global digital elevation model with two distinct satellites, thus requiring a coordinated operation of the two satellites formation. To achieve this precise motion, a HELIX formation was chosen, as this type of architecture enables a safe operation of the satellites without implementing autonomous controls. This lack of controls derives from the two satellites different motion. By having an out-of-plane orbital displacement with different ascending nodes, and implementing a radial separation with different eccentricity vectors, the depicted formation scheme presents no risk of orbital crossing, thus no collision risk between the formation elements.

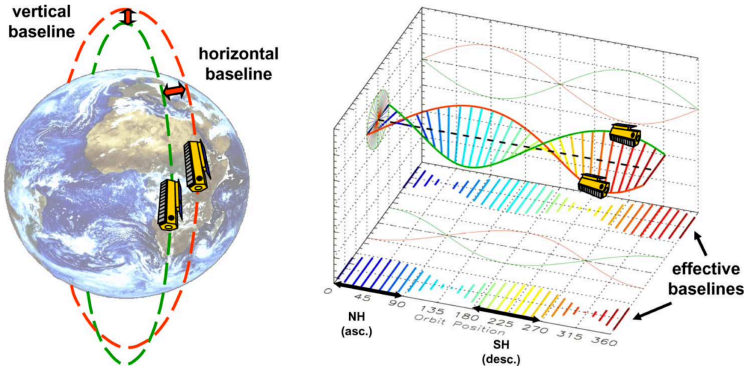

Figure 2.3: Orbit Tracking formation strategy example (Adapted from [21])

- Leader/Follower: this approach implies having a central satellite, denoted as the leader whose only purpose is the constant maintenance of its motion in the reference orbit whilst the other satellites, the followers, are responsible to continually correct their trajectories relative to the leader. This strategy enables the leader satellite to independently follow the chosen orbital path with the follower element being the only responsible of the two satellites relative motion correction, therefore representing a simpler relative state control implementation. Despite this obvious advantage, the leader/follower approach entails the unevenness of the fuel consumption, between the leader's and the followers orbital actions [11]. Both TechSat 21 and PRISMA missions are examples of configurations following a Leader/Follower formation scheme [17], [22]. About TechSat 21 mission, this was a formation flying demonstrator with the purpose of achieving circular, near-circular, and J_2 invariant relative trajectory's configurations. Throughout the mission, these demonstrations validated the millimeter level precision of these architectures while applying control approaches defined for fuel consumption

and expenditure minimization. PRISMA project was a similar project once it was also a technology demonstration mission. Like the previously described mission TechSat 21, the PRISMA mission was designed to validate the implementation of formation flying configurations maintenance and in-orbit servicing, by adopting a Leader/Follower strategy, i.e. it consisted of a smaller target satellite passively moving in a 700km orbit altitude and a maneuverable minisatellite. This mission provided valuable information concerning onboard systems and configuration autonomy, robustness, safety, and formation precision, thus also validating the usage of this formation strategy and reinforcing the overall usage of formation flying technology[17], [22].

- Virtual Structure: is a formation scheme where the craft in the formation are viewed as a rigid body. The overall relative positioning and placement of the satellites in the configuration is previously defined, thus all elements in the formation move as a single structure. Throughout the mission lifetime the sole purpose of the control scheme is the formation shape maintenance, therefore moving as a single ”virtual structure” resultant from the group’s coordinate motion management. However, this approach needs constant coordination and an inter-spacecraft communication for the formation maintenance, which implies a more complex control implementation than the previously referred approaches. There are missions like PROBA-3, Fig. 2.4, where a virtual structure scheme formation not only offers a low-budget substituting to the currently used technology, but also enhance their presently limited performance by offering a whole new scope of possibilities [23]. This mission objectives will be the incorporation of the ASPIICS(Association of Spacecraft for Polarimetric and Imaging Investigation of the Corona of the Sun - a solar coronagraph formation flying mission developed by ESA) in a formation flying configuration, thus conceiving a externally-occulted solar coronagraph intended to observe the coronal base with high resolution equipment. Composed by two platforms separated by about 150m, the coronagraph hosted by one spacecraft remains entirely protected from the direct sunlight by remaining in the shadow of the external occulter hosted by the other spacecraft. This formation flying concept will open a new era of high quality imaging of the inner corona up to now inaccessible and represented a first step toward more ambitious solar missions using formation flying and the virtual structure schemes [23].

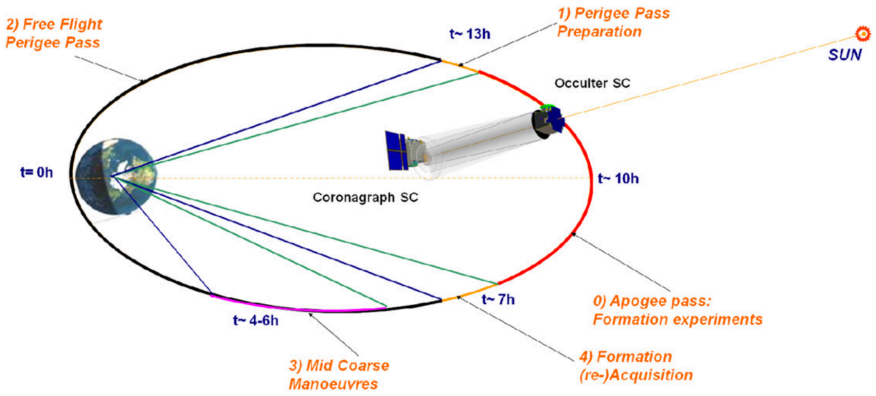

Figure 2.4: Virtual Structure formation strategy example (Adapted from [24])

- Swarm: also called as behavioral approach, this formation configuration works through the arbitrary arrangement of a large number of satellite inside a specified limited volume, where the satellites arrange their motion based on their peer's local information. The relative control action is performed individually. This overall formation control action can be determined by a weighted average of the configuration necessary control corrections. This kind of method represents an advantageous approach when considering missions with a large number of satellites, once it requires lower computer burdens generally. Nevertheless, it demands intricate collision avoidance algorithms and it requires a high fuel consumption far from the optimal values. The satellite swarm method is suitable for situations where the control system has multiple, and sometimes competing objectives or behaviors. Behaviors could include goal attainment, collision avoidance, obstacle avoidance and formation keeping. This method is used in [25] where the authors developed a collision avoidance algorithm based on this behavioral approach. In this study the objective is to develop an algorithm capable of controlling a swarm-type formation of 3U CubeSats that could achieve the required spatial distribution in the along-track direction by controlling their attitude and using solely the differential drag force.

Along with the controlling schemes and strategies, it is also important to take into account the environmental disturbances that influence the expected motion of the orbiting bodies. When considering Low-Earth-Orbits (LEO), there are some influencing external factors such as atmospheric drag, solar radiation pressure, the perturbation effects of the Earth's gravity due to its oblation, are just a few effects that shall be considered through the mission design process and which have most influence. In the [26] study, the authors developed a control algorithm for a satellite formation flying placed at a Low-Earth-Orbit (LEO), accounting the Earth oblateness J_2 and the atmospheric drag effects. The algorithm developed is a corrector that is expected to compensate the formation's relative drift, caused by both J_2 and drag perturbations. The simulation results prove the control effectiveness by reaching the relative drift values to the minimum, however the drift is not completely eliminated, which proves

the difficulty of successful elimination of these perturbations [26].

Thus, it is therefore needed to account for the influence of several external forces along with the development of the control algorithm. This environmental disturbances are compensated by an on-board propulsion systems, which require the application of methods to minimize the fuel expenditure. Fuel-based control systems, besides requiring a long development phase and implementation study, also require the existence of additional payload room for the fuel storage tanks. However, instead of trying to eliminate the influence of these external forces, it is possible to rely on them and even use them as the control source, as it is studied in [27], [28], [25] cases. Differently from [28] and [25] studies that consider an approach where the atmospheric drag force is used as the formation control source, in [27] the authors develop a control algorithm based on the utilization of the solar radiation pressure acting on the satellites in a LEO. In this paper, the respective solar sails are made of a special type of material with an optical changing abilities. This characteristic enables the two spacecraft in the system to control both the relative orbital motion and the single satellite attitude by changing the overall solar pressure influence on each solar sail. Therefore, by achieving the appropriate pattern of black and white cells in the sail, the developed control scheme allows the control of the relative motion for the two satellites' formation using solely a solar sail system with variable optical properties only. However, it has been shown that the use of this system is only suited for time intervals when the Clohessy-Wiltshire approximation is valid and for solar sails with a minimum number of sixteen individual cells [27].

In papers [25] and [28] the developed control algorithm is based on the utilization of the atmospheric drag force exerted on the satellites in the formation system. The first study considers a simple aerodynamic force model that accounts with the lift component caused by the rigid interaction between the satellite's surface and Earth's atmospheric molecules. By calculating the satellite's attitude relative to the incoming flow, the required force for the formation control is provided through a control that accounts not only with the inaccuracy of the atmospheric density model but also the J_2 effect from the Earth's gravitational field. The application of this control algorithm is validated through the numerical simulations conducted. The algorithm is able to control the spacial distribution of the formation in a three-dimensional relative motion, ensuring a control capable of achieving the required trajectory (with a deviation close to zero) [28]. Similarly, paper [25] also considers a control based on the atmospheric aerodynamic drag effect, but this time for a swarm formation concept. The goal of this study is the development of a decentralized control algorithm capable of providing convergence of the relative drift of all the satellites in the swarm to the vicinity of zero. The authors consider then a swarm composed of 3U CubeSats (a shape that is best suited for this type of control due to its form factor) in a LEO subjected to the J_2 gravitational effect and to the Earth's atmosphere modeled after the GOST model. The numerical simulations prove the effectiveness of this type of control for three different swarm configurations (compact, motion in a restricted area and uniform distribution in the along-track direction) and despite the low accuracy of the satellites stabilization relative to the incoming airflow the relative trajectories become limited. Along with the translational and attitude motion control, a

collision avoidance system based on the drag effect is also implemented. This collision avoidance algorithm is activated only in cases where a second satellite enters inside a determined dangerous collision area, being implemented a differential drag in both satellites to increase the nearest relative distance [25].

Approaches for formation flying control exploiting the external/environmental elements are taking wider interest in the current days. These approaches shall imply fuel-free satellites with more room for mission primary payload. Aligned with this scientific chain, this dissertation was developed, based on Lorentz force studies and which are examined in the next section.

Further, another key studies considering a wide diversity of formation flying aspects are examined in the papers [16], [6], [29] and [15], studies that were considered in the development of the control algorithm addressed in this dissertation but were not thoroughly described in this section for the sake of keeping it concise and brief.

2.3 Overview of the Lorentz force works

A charged particle, which is moving with a determined velocity relative to the Earth's magnetic field, accelerates in a direction perpendicular to its velocity vector and the local magnetic field vector due to the Lorentz force, an effect represented in Fig(2.5) [30]. The application of this force for a spacecraft formation flying control is a relatively new idea and, therefore a rather unstudied one. The first works about the Lorentz force effects on charged bodies were conducted by Schaffer and Burns who developed a model explaining the influence of the plasma environment on the dynamics of charged dust particles orbiting Jupiter and Saturn [31]. These studies proved that the orbital motion and dynamics are greatly influenced by the Lorentz force and that this magnetic force along with gravity effects, lunar perturbations, and solar pressure are responsible for the existence of gaps in both Jupiter's and Saturn's ring resonances. These works represented a valuable contribution to validating models concerning the charging of particles and the demonstration that Lorentz force effects lead to non-Keplerian orbits [31].

Following the work developed by Schaffer and Burns, Peck conducted a series of studies proposing the implementation of the Lorentz force for the development of a propellantless satellite technology. In paper [30] Peck explores the development of LAO (Lorentz-Augmented Orbit) system which could be capable of using this effect for orbital control. It also provides a wide range of LAO systems that would be solutions for Earth escaping, drag compensation, formation flying control, inclination control, nodal precision control, new sun-synchronous and even non-Keplerian polar orbits. This Lorentz force effect is experienced individually by any charged spacecraft and, in contrast to Coulomb force, it is not resultant from the interaction between two charged spacecraft. Instead, this force is caused by a magnetic interaction between the charged spacecraft's relative velocity and the environ-

ments magnetic field. Both the direction and magnitude of the Lorentz force are a function of the satellite's orbital motion (presenting different values for different orbital positions and therefore being sensible to the orbits geometry), being its direction always perpendicular to the spacecraft's velocity and the local magnetic field vector.

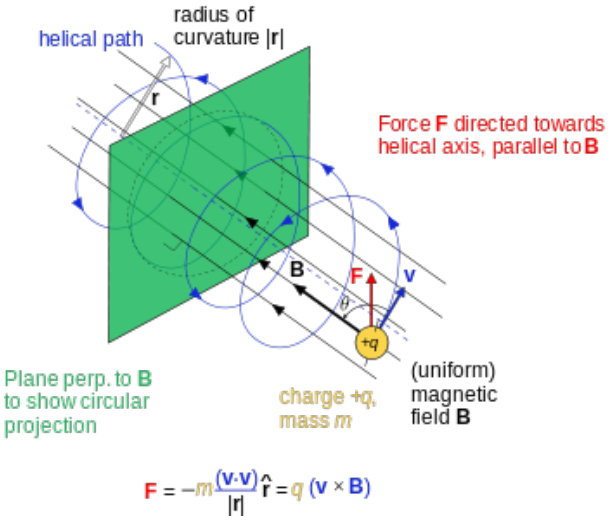

Figure 2.5: Representation of the Lorentz force acting on a charged particle. (Credit from [32])

Peck [30] also presents a possible design for LAO system configurations, Fig. 2.6. Although LAO system configurations does not involve the use of electrodynamic tethers, the operation physics of both devices are similar. For a LAO spacecraft, the body acts as a point charge which moves with a velocity of thousands of meters per second relatively to the planet magnetic field. The moving charge represents the current similar to the one acting in electrodynamic tethers [13].

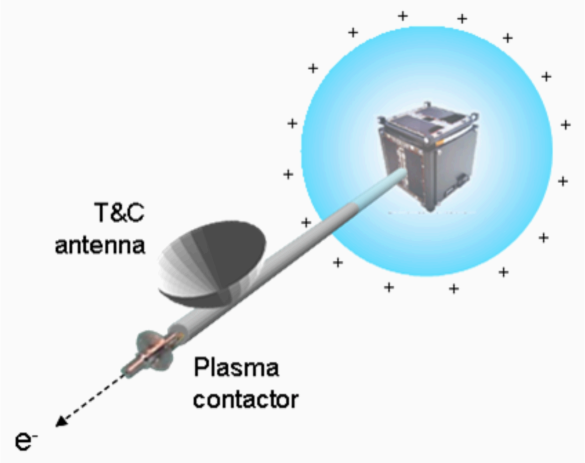

Figure 2.6: Example of a possible configuration for a LAO satellite proposed by Peck (Credit from [30])

LAO equipped spacecraft formations are not designed to control their motion via attractive or repulsive forces, in contrast to the systems described in [12] and [33] papers. In the paper [33] the authors examine the possibilities the Electromagnetic Formation Flying systems (EMFF) for nearby satellites inspection possibilities. These inspections would be performed by a group of three satellites, each one capable of controlling both their attitude and relative position, individually, inside the formation by driving a current through a set of three magnetic coils [33]. Thus, the formation motion control is performed by this magnetic dipole creation enabling the relative state control of each formation element. This magnetic interaction offers increased control, guidance, and navigation capabilities. Another study that focused on the replacing of large fuel-based systems by embracing a formation flying scheme is [12]. This study gives an alternative technology for NASA's Terrestrial Planet Finder (TPF) mission, based on the application of a multiple spacecraft with electromagnetic control capabilities. Focusing on the elimination of secondary effects associated with propellant-based systems, such as fuel depletion, optical contamination, or plume impingement, the authors develop an optimized electromagnetic system capable of replacing the more traditional fuel-based control options. The application of electromagnetic forces, such as the Lorentz force, enables systems like TPF to control the relative translational motion and attitude, as well as the inertial rotation of the formation. As the authors concluded, EMFF system concepts represent the most attractive options for this type of mission, especially when long mission lifetimes are considered (in theory, the proposed EMFF system is able to operate indefinitely, or at least until the component failure). A characteristic that when allied with the propellantless possibilities reinforces the viability of EMFF mission concepts [12].

Another major aspect to account when developing a LAO system, namely during the simulation of the system operation is the Earth's tilted magnetic dipole feature. This Earth magnetic model is widely used in numerous studies involving the implementation of Lorentz control systems, including the study [34]. This paper goal is to examine the application of the Lorentz force as the orbital maneuvering control of a charged spacecraft, but also to demonstrate the utilization of such electromagnetic forces for the construction and reconfiguration of formation flying configurations. By studying and comparing the formation flying control considering a tilted and a non-tilted dipole model, the authors conclude that without considering the tilted dipole feature it is not possible to use the Lorentz force as a mean for the formation motion control. Due to the geometric interaction between magnetic field and velocity vectors, the dipole's rotation axis inclination feature, even if small, allows the control of the satellites relative motion in contrast to a situation where this feature is nonexistent. Thus, as proved by the simulation results in [34], the adoption of a tilted dipole model is a crucial step to obtain reliable and adequate results when simulating LAO systems. These results are not affected when considering a more complex geomagnetic model, such as the IGRF, once the added precision of this model (compared to the tilted dipole model) do not influence the the correct functioning of the control algorithm studied.

The Lorentz electromagnetic force has been widely studied for several applications, not only considering the formation flying control but also a set of satellite control problems, as in

the case of [35] where the authors propose a Lorentz-based control scheme for the attitude control of a spacecraft in LEO. In this paper, the authors goal is the development of a pitch and roll direction torques electromagnetic controller that could replace the traditional attitude control systems. However, the authors were forced to consider an elliptical orbit as a way of introducing a varying relative motion between the satellite and the Earth's magnetosphere, once a non-tilted dipole model was considered during the simulations [35]. Another example of a LAO controlled spacecraft development is the paper [36] case, presenting the development of a new propellantless orbital control system. By executing two different time varying studies, considering one-day-averaged and single-orbit-averaged approaches, the authors realise that after a 24 hour period a corrector must be applied to counter both J_2 and Lorentz influence on three of the six classical orbit elements. To perform these studies, a new model that bounds a Lorentz-augmented orbit with a J_2-invariant perturbations models is successfully developed and simulated [36]. The orbital transfer case and the orbital maneuvering for single satellites as well as for satellite formations is also studied in [37], [38] and [34]. While opting for the development of a hybrid system (a Lorentz acceleration system allied with a thruster-generated system) and a nonlinear dynamical model scheme for the maneuver control [34], the authors proposed new control schemes that proved to be effective. The positive results were obtained not only for elliptical orbits cases but also for alternative Lorentz-augmented relative orbital situations. This control scheme adaptive profile is also considered in the [38] study case, where the developed algorithm for a formation control situation is successfully applied for an orbital transfer.

Chapter 3

Orbital Dynamics and Environment Characterization

Orbital dynamics is a subject responsible for describing and predicting the motion of orbiting bodies and their respective attitude in the space environment, considering both artificial and natural forces acting acting on it and affecting the orbital motion. These analysis takes into account all the prevailing factors that could influence the general motion of orbiting bodies. As so, the orbital dynamics analyses and the respective operation assessment represent a major aspect in the development of satellite missions [39], [40], [41].

This chapter aim is to address formation flying dynamics fundamentals and respective equations for relative motion control problem description, considering the main perturbations and errors associated both with launching conditions and the orbital environment.

3.1 Two-Body Problem

The two-body problem is a formulation whose purpose is to model the motion of two co-rotating points masses, in a given reference frame, where the gravitational attraction between the two bodies is the sole force acting on the system [40], [7].

Consider $\mathbf{R_1}$ and $\mathbf{R_2}$ as the position vectors of two bodies with mass m_1 and m_2 respectively, represented in a three-dimensional inertial frame of reference denoted by $OXYZ$, Figure 3.1, and expressed as follows

$$\mathbf{R_1} = X_1\mathbf{i} + Y_1\mathbf{j} + Z_1\mathbf{k}, \tag{3.1}$$

$$\mathbf{R_2} = X_2\mathbf{i} + Y_2\mathbf{j} + Z_2\mathbf{k}, \tag{3.2}$$

$$\mathbf{r} = \mathbf{R_2} - \mathbf{R_1}. \tag{3.3}$$

and where the indexes $\mathbf{i}$, $\mathbf{j}$ and $\mathbf{k}$ come after the unit vectors of the axis in the reference frame $OXYZ$, respectively [42].

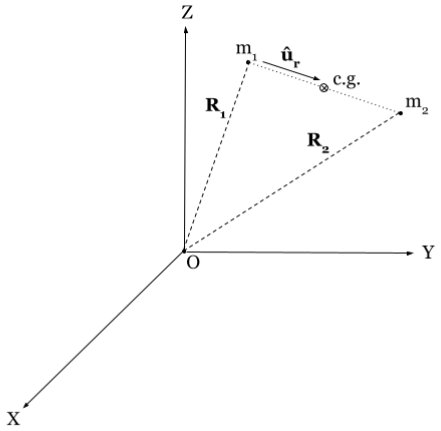

Figure 3.1: Inertial frame of reference.

The two bodies center of mass can therefore be represented by the vector $\mathbf{r_c}$,

$$\mathbf{r_c} = \frac{m_1\mathbf{R_1} + m_2\mathbf{R_2}}{m_1 + m_2}. \tag{3.4}$$

The resultant gravitational attraction, acting upon both bodies, which operates along the line that joins their centers of mass, is given by

$$\mathbf{F_{12}} = \frac{Gm_1m_2}{r^2}\hat{\mathbf{u}}_\mathbf{r}. \tag{3.5}$$

where G represents the universal gravitational constant, r corresponds to the magnitude of the vector $\mathbf{R}$ and $\hat{u}_r$ is the unit vector pointing from the body with m_1 mass towards the second body with mass m_2. All of this vectors are presented in Figure 3.1.

Using Newton's second law of motion, i.e., $\mathbf{F} = m\mathbf{a}$ (where a denotes the instantaneous body acceleration), and combining it with Newton's general gravitation law, the previous (3.5) can then be rewritten as

$$m_1\ddot{\mathbf{R}}_\mathbf{1} = \frac{Gm_1m_2}{r^2}\hat{\mathbf{u}}. \tag{3.6}$$

where $\ddot{\mathbf{R}}_1$ denotes the absolute acceleration value of the body with mass m_1.

After Newton's third law, or the action-reaction principle, the acting force on m_2 can be described as

$$\mathbf{F}_{21} = -\frac{Gm_1m_2}{r^2}\hat{\mathbf{u}}_r. \tag{3.7}$$

which, by combining it with (3.5) and having opposite signs results in the equality

$$m_1\ddot{\mathbf{R}}_1 + m_2\ddot{\mathbf{R}}_2 = 0. \tag{3.8}$$

From this relation it is then possible to deduce that the acceleration of the system's center of mass is constant and equal to zero, relative to the origin of the $OXYZ$ inertial frame [39], [42].

Dividing out (3.6) by the body's mass m_1, and following the same principle for the second body in the system, the equations are then rearranged as

$$\ddot{\mathbf{R}}_1 = -Gm_2\frac{\mathbf{r}}{r^3}, \tag{3.9}$$

$$\ddot{\mathbf{R}}_2 = Gm_1\frac{\mathbf{r}}{r^3}. \tag{3.10}$$

which results in the reformulation of equations 3.3 and 3.4 in

$$\ddot{\mathbf{r}} = \ddot{\mathbf{R}}_2 - \ddot{\mathbf{R}}_1, \tag{3.11}$$

$$\ddot{\mathbf{r}} = -\frac{G(m_1 + m_2)}{r^2}\hat{\mathbf{u}}. \tag{3.12}$$

where $\ddot{\mathbf{r}}$ corresponds to the relative acceleration vector.

The term μ represents the gravitational parameter and can be defined as follows

$$\mu = G\left(m_1 + m_2\right), \tag{3.13}$$

which can therefore be applied in (Eq.3.12) standing

$$\ddot{\mathbf{r}} = -\frac{\mu}{r^3}\mathbf{r}, \tag{3.14}$$

Assuming that $\mathbf{h}$ defines the relative angular momentum of a body per mass unit, i.e., the specific angular momentum,

$$\mathbf{h} = \mathbf{r} \times \dot{\mathbf{r}}, \tag{3.15}$$

$$\frac{d\mathbf{h}}{dt} = \dot{\mathbf{r}} \times \dot{\mathbf{r}} + \mathbf{r} \times \ddot{\mathbf{r}}, \tag{3.16}$$

from which (3.16) stands as $\mathbf{h}$ time derivative. Knowing that $\ddot{\mathbf{r}} \times \ddot{\mathbf{r}} = 0$, and operating the substitution

$$\ddot{\mathbf{r}} = -\frac{\mu}{r^3}\mathbf{r}, \tag{3.17}$$

an expression that results in $\frac{d\mathbf{h}}{dt} = 0$ and from which is possible to derive the conservation of angular momentum for a two-body system and to verify that the cross-product resultant vector remains normal to the orbital plane.

3.2 Orbital Elements

Kepler formulated three rules for a two body problem to describe the motion of orbiting bodies in a two dimensional plane [11], [40], [41]:

- 1st law: the planet's orbits form ellipses, being one of the two foci located at the Sun.
- 2nd law: considering the existence of a line segment joining a planet and Sun center, this line takes equal time intervals to sweep out equal areas.
- 3rd law: the cube of the orbital semi-major axis length is proportional to the square of a planet's orbital period.

The six constants, also referred to as classical orbital elements or Keplerian elements, are capable of describing either the position and the velocity of a certain orbiting body along its trajectory. These six parameters defined by the initial conditions, represent different trajectories, which are represented in Figure 3.2: two orbital parameters describe the orbit shape and size, three define the orbital plane attitude and a last one describes the satellite trajectory connection with current time [40], [41]. Below are enumerated the seven parameters most commonly used.

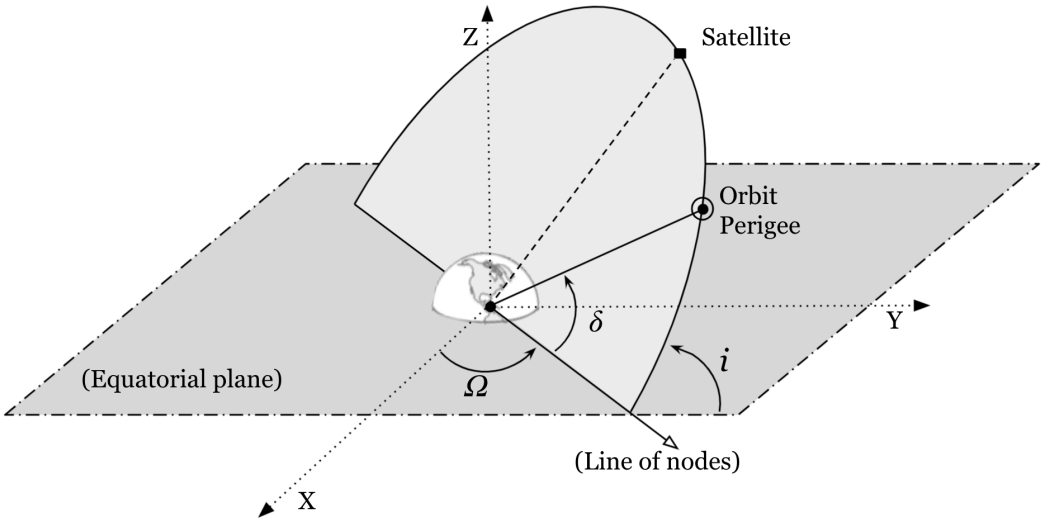

Figure 3.2: Orbital elements representation.

- Semimajor Axis (a) - The semimajor axis is the parameter that defines the orbit size. So, for a spacecraft orbiting Earth in a circular orbit the semimajor axis is calculated as a sum of the altitude (h) of the spacecraft with the Earth radius, while for an elliptical orbit the semimajor axis is half of the major axis.

- Eccentricity (e) - The eccentricity is the parameter that depicts the orbit shape, calculated dividing the distance between the ellipse center and its focus by the semimajor axis. For a circular orbit, the eccentricity value is $e = 0$, as for an elliptic orbit the eccentricity value is somewhere placed inside the $0 < e < 1$ interval. Parabolic and hyperbolic trajectories eccentricity values are $e = 1$ and $e > 1$, respectively.

- Inclination (i) - The inclination describes the orbital plane orientation in space. It is defined as the angle between the orbital plane and the equatorial plane.

- Right Ascension of the Ascending Node (Ω or $RAAN$) - This is an angle measured between the OX axis and the ascending node direction. The line of the nodes is the name given to the connecting segment established between the ascending node (point in equatorial plane where the satellite crosses the equator from south to north) and the descending node (point at which the equatorial plane is crossed form north to south by the satellite).

- Argument of Perigee (δ) - The parameter responsible for the position of the ellipse in the orbital plane. This angle is measured from the Ascending Node to the radius-vector of orbital perigee.

- Time of perigee passage (τ) - This is an often used alternative to the True anomaly to describe the satellite trajectory connection with the current time. This parameter is defined as the the time instant on which the satellite is at the orbital perigee.

Along with these six constants there is also another parameter frequently used when dealing with a satellites orbital motion called true anomaly (θ), which is responsible for the satellite location within the orbit. It is an angle measured in the satellite's motion direction, from the perigee to the current orbital position.

3.3 Reference Frames

The definition of a suitable reference frame is one of the first steps to account to describe and study an orbit. Any problem concerning kinematics, changing rates, or physical quantities require a basis establishment from where these rates can be measured and referred, giving rise to coordinate systems, i.e., any trajectory in a dynamical system must be expressed accordingly to a defined reference frame [11], [41].

Consider the following reference frames, Fig. 3.3, 3.4 and 3.5:

- ECI, or Earth Centered Inertial, is a cartesian system whose origin is coincident with Earth's center of mass. The X-axis is then directed from this center along with the vernal equinox (the Aries constellation), while the Z-axis is normal to the equatorial plane and points towards the geographic north pole (defined as the positive direction and which is coincident with the Celestial Ephemeris Pole - CEP), and with the Y-axis completing the right-handed orthogonal triad lying in the equatorial plane.

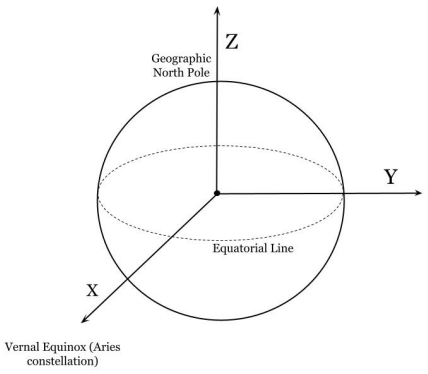

Figure 3.3: ECI reference frame.

- ECEF, or Earth Centered Earth Fixed, is a rotating coordinate system with its center coincident with the Earth's. The $\hat{x}$ unit vector is defined through a line from the referential origin to the intersecting point in the Earth's surface with 0° latitude and 0° longitude, while the $\hat{z}$ is parallel to the Earth's geographic north and the $\hat{y}$ completes the triad.

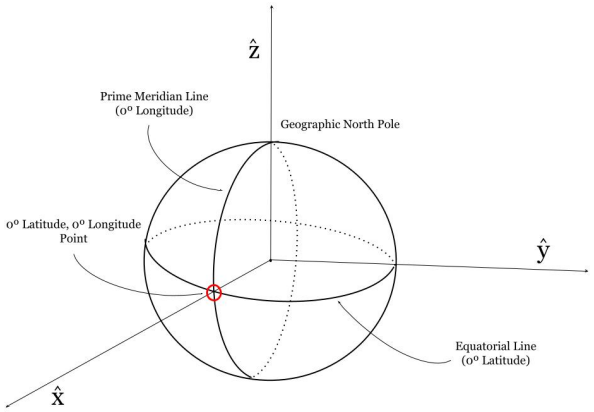

Figure 3.4: ECEF reference frame.

- Hill frame, also called Local Horizontal Local Vertical, is a rotational coordinate system whose origin is centered at a reference point along the orbital plane (usually the spacecraft). With z-unit vector directed from the reference point along the radius vector from the Earth center through the reference frame origin, the y-axis direction is established along the orbital momentum vector (normal to the orbital plane) and the x-axis completes the triad.

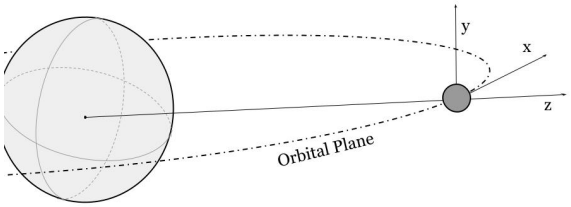

Figure 3.5: Hill reference frame.

The spacecraft's body-fixed frame is not considered throughout this work, once the main focus is the orbital relative trajectory control. Concerning this, only the relevant reference frames were described, whereas others can be found in [2][3].

3.4 Reference Frame Conversion

After the reference frames definition, it is now required to establish the relation and the conversion methods from one to another. Through coordinate rotation sequence (angle rotations called Euler angles), it is possible to express a vector's component in an alternate reference system and therefore providing the possibility of describing a new types of motion [11].

From the initial reference state vector it is possible to define the Keplerian orbital elements. The calculated satellites control functions are expressed in the LVLH reference, while for the simulation the orbital motion is expressed in the ECI frame. It is therefore necessary to explicit these transformations from one motion frame representation into another [11], [40].

The following subsections will summarise the coordinate transformations between the considered reference frames.

3.4.1 OE to ECI

The conversion from the Keplerian Orbital Elements, Fig. 3.2, into the position **R** and velocity **V** vectors, represented in the ECI frame, Fig. 3.3, begins by calculating the semi-latus rectum p, and the M value representing the orbital mean anomaly [1][4]:

$$p = a\left(1 - e^2\right) \tag{3.18}$$

$$b = \sqrt{ap} \tag{3.19}$$

$$M = \sqrt{\frac{\mu}{a^3}}\left(t - t_p\right) \tag{3.20}$$

where the variable a is the semimajor axis of the ellipse, b is the semiminor axis, e the ellipse eccentricity value, while t and t_p represent the current and the passage time at the periapsis (τ), respectively. As the time origin reveals to be arbitrary, the current time could be measured as starting at the periapsis passage time, i.e, $t_p = 0$. Thus, from the mean anomaly value it is possible to calculate the eccentric anomaly E from the following equation,

$$E - e\sin E = M \tag{3.21}$$

This is a transcendental equation whose solution can only be solved applying iterative numerical methods such as Newton's method. Assuming $E = 0$ as the initial value, the eccentric

anomaly is calculated using the following procedure

$$E_{n+1} = E_n - \frac{E_n - \sin E_n - M}{1 - e\cos E_n} \tag{3.22}$$

where n represents the iteration number. The procedure is stopped when ($||E_{n+1} - E_n||$) achieves the required value. Following the eccentric anomaly determination, then it is possible to calculate the true anomaly value using the following equations

$$\cos\theta = \frac{\cos E - e}{1 - e\cos E} \tag{3.23}$$

$$\sin\theta = \left(1 - e^2\right)^{\frac{1}{2}} \frac{\sin E}{1 - e\cos E} \tag{3.24}$$

These values are then applied in the following equations,

$$\upsilon_r = (\frac{\mu}{p})^{\frac{1}{2}} e\sin\theta \tag{3.25}$$

$$\upsilon_n = (\frac{\mu}{p})^{\frac{1}{2}}(1 + e\cos\theta) \tag{3.26}$$

where μ stands as Earth's standard gravitational parameter, θ represents the true anomaly (angle measured in the orbital plane between the perigee point and the ascending node position). The parameters υ_r and υ_n denote the radial and normal velocity, respectively. The initial position, R_o, and velocity, V_o, vectors expressed in the ellipse principal axes are as follows

$$\mathbf{R_o} = \begin{bmatrix} a\,(\cos E - e) \\ b\sin E \\ 0 \end{bmatrix} \tag{3.27}$$

$$\mathbf{V_o} = \begin{bmatrix} \upsilon_r \cos\theta - \upsilon_n \sin\theta \\ \upsilon_r \sin\theta + \upsilon_n \cos\theta \\ 0 \end{bmatrix} \tag{3.28}$$

The initial absolute position and velocity vectors, in ECI frame are therefore calculated relying on the Euler angle transformation sequence, defined using the following direction cosine matrices

$$A_1 = \begin{bmatrix} \cos\Omega & \sin\Omega & 0 \\ -\sin\Omega & \cos\Omega & 0 \\ 0 & 0 & 1 \end{bmatrix} \tag{3.29}$$

$$A_2 = \begin{bmatrix} 1 & 0 & 0 \\ 0 & \cos i & \sin i \\ 0 & -\sin i & \cos i \end{bmatrix} \tag{3.30}$$

$$A_3 = \begin{bmatrix} \cos\delta & \sin\delta & 0 \\ -\sin\delta & \cos\delta & 0 \\ 0 & 0 & 1 \end{bmatrix} \tag{3.31}$$

Thus, the satellite's position and velocity vectors in ECI are expressed as follows

$$\mathbf{R_i} = \left[A_3 A_2 A_1\right] \mathbf{R_o} \tag{3.32}$$

$$\mathbf{V_i} = \left[A_3 A_2 A_1\right] \mathbf{V_o} \tag{3.33}$$

$$\begin{aligned} \mathbf{X_i} &= \left[\mathbf{R_i}, \mathbf{V_i}\right]^T \\ &= \left[X, Y, Z, \dot{X}, \dot{Y}, \dot{Z}\right]^T \end{aligned} \tag{3.34}$$

where the index **i** stands for the satellite numeration, and thus $\mathbf{X_i}$ denotes the state vector of the satellite.

3.4.2 ECI to HILL frame

For the relative motion equations development process, a second transformation is essential to obtain the relative state vectors for each of the satellites in the Hill frame. The orbital point is taken as the reference frame origin for the Hill frame.

Hill rotating frame can be obtained following the equations bellow,

$$\mathbf{x}' = \mathbf{y}' \times \mathbf{z}' \tag{3.35}$$

$$\mathbf{y}' = \frac{\mathbf{R_i} \times \mathbf{V_i}}{||\mathbf{R_i} \times \mathbf{V_i}||} \tag{3.36}$$

$$\mathbf{z}' = \frac{\mathbf{R_i}}{||\mathbf{R_i}||} \tag{3.37}$$

where the operator ($\times$) stands for the cross product of the satellite's position and velocity vectors expressed in ECI. Combining this axis direction vectors in a matrix A, a general rotation matrix for the frame's transformation is obtained:

$$A = \left[\mathbf{x}', \mathbf{y}', \mathbf{z}'\right]^T \tag{3.38}$$

The orbital angular velocity (Φ) is presented below:

$$\Phi = \frac{\mathbf{R_i} \times \mathbf{V_i}}{||\mathbf{R_i}||^2} \tag{3.39}$$

from which is possible to denote that Φ is perpendicular to the orbital reference plane and points out in the same direction as the orbital momentum, and whose expression.

The equation for the relative motion state vector consisting of the relative position vector r_{ab} and relative velocity v_{ab} expressed in Hill frame is as follows:

$$\begin{aligned} \mathbf{x_{ab}} &= \left[A(\mathbf{R_b} - \mathbf{R_a}), A(\mathbf{V_b} - \mathbf{V_a}) - A\left(\Phi \times (\mathbf{R_b} - \mathbf{R_a})\right)\right]^T \\ &= \left[\mathbf{r_{ab}}, \mathbf{v_{ab}}\right]^T \\ &= \left[x'_{ab}, y'_{ab}, z'_{ab}, \dot{x}'_{ab}, \dot{y}'_{ab}, \dot{z}'_{ab}\right] \end{aligned} \tag{3.40}$$

where the indexes a and b represent each of the elements in a two satellite formation flying.

3.5 J2 Gravity Model

The problem associated with Keplerian laws of motion is the fact that the calculated orbital description is based in the assumption where the intervening bodies have a symmetric mass distribution and a spherical shape. Consequently, these equations discard any external force acting on the bodies apart from the Earth central gravity and therefore it is needed to correct these equations to take into account other factors acting on the orbiting bodies [11]. Taking into consideration Earth's true mass distribution, third bodies gravitational forces, atmospheric drag force, or the solar pressure effect all have an influence on orbital motion and an impact on its elements [43].

This section aims to describe the gravitational model used for the motion simulation. It should be noted that considering the objective of the conducted study, perturbations caused by third bodies' gravitational influence and aerodynamic drag were not considered in the paper.

Even though often being modeled as spherical, Earth is a complex non-spherical body with a non-uniform mass distribution. It has a bulge in the equatorial zone and a flattening at the poles area that results in a non-centered gravitational field. Also considering Earth's surface irregular geography (topography diversity such as mountains ranges) and the consequent non-uniform mass distributions, numerous models for the mass representation were created. The geoid or the ellipsoidal models are some examples (Fig.3.4).

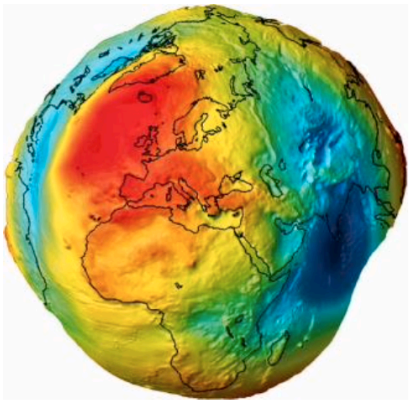

Figure 3.6: The Earth geiod represented in an exaggerated scale.(Adapted from [44])

The ellipsoidal gravitational model, widely used for semiprecise calculations, assumes the Earth shape as an oblate spheroid with the semimajor axis equal to the equatorial radius and the semiminor axis coincident with the polar radius line. This model is composed of a set of coefficients in the spherical harmonic expansion, mathematical terms directly derived from the Earth's gravity potential. The coefficient of the second harmonic is con-

sidered in this paper and it represents the largest of the geopotential terms. This J_2 effect takes an influence in the secular variation of Ω and the δ orbital elements. This effect occurs mainly due to the "Earth oblateness", the equatorial bulge resultant from the radius difference between the poles and the equatorial zone and is represented with the constant value of $J_2 = 1.75553 \cdot 10^{10}(km^5 s)$. The effect of this disturbance on the body acceleration and is calculated as follows:

$$a_{J_2} = \delta_{J_2} \frac{1}{R_i^5} \left(1 - \frac{5z^2}{R_i^2}\right) \begin{bmatrix} X, & Y, & Z \end{bmatrix} \tag{3.41}$$

$$\delta_{J_2} = \frac{3}{2} R_E^2 \, \mu \, J_2 \tag{3.42}$$

$$J_2 = 1.75553 \cdot 10^{10} \tag{3.43}$$

where the Z element represents the z-axis component of the position vector in ECI and R_E is the equatorial Earth radius with the value of $R_E = 6.378 \times 10^6 m$.

3.6 Dipole Geomagnetic Model

Besides the gravity potential model, it is also important to define Earth's geomagnetic field environment. This model is crucial for this study, once this work objective is to develop a formation control using solely the Lorentz force. Since this is a force of electromagnetic nature, it is needed to simulate the Earth's magnetosphere.

For the simulation of the Earth magnetosphere there are several models, with different precision values accordingly to the observation methods and to the correspondent period of measurements. Models like the International Geomagnetic Reference Field (IGRF), CHAOS-7 or LCS-1 are frequently used when a high degree of precision is needed in cases where the small variations of the Earth magnetic filed values could signify undesirable manifestations on the mission's objective [45], [46].

However, due to their high precision magnetic field variation data, these models take a large numerical calculation steps, which in the case of this study would mean a more complex simulation stage. Therefore, a simpler generic model was adopted, the Tilted Dipole Geomagnetic Model Fig. 3.7 [36], [47]. Despite being considered a "raw" simulation of the real Earth Geosphere, this is rather easy to implement computationally and, although providing low precision data, it matches the precision needed for this technology validation study.

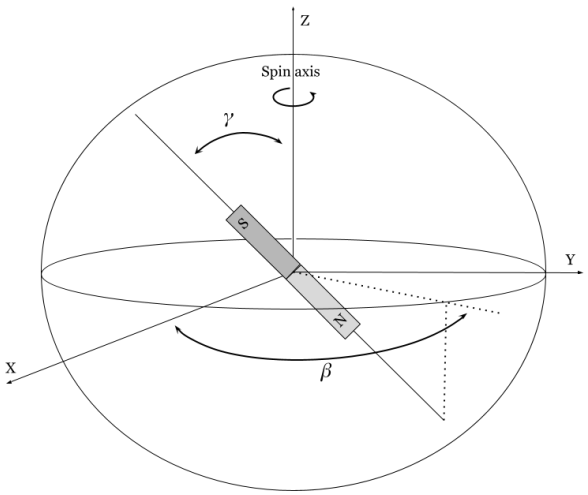

Figure 3.7: Earth's geomagnetic model considered - tilted dipole geomagnetic model.

Considering the propositions stated above, and based on the electrodynamics classical theory, the Earth's magnetic model B and its Electric Field model E are defined as

$$\mathbf{B} = \frac{B_o}{r^3}\left[3(\hat{\mathbf{N}} \cdot \mathbf{R_i})\mathbf{R_i} - \hat{\mathbf{N}}\right] \tag{3.44}$$

$$\mathbf{E} = -(\tilde{\omega} \times \mathbf{r}) \times \mathbf{B} \tag{3.45}$$

where R_i corresponds to the spacecraft position unit vector and r its magnitude, B_o is the Earth magnetic dipole moment with the value of $B_o = 8 \times 10^6 (T k m^3)$, and the $\hat{\mathbf{N}}$ parameter defining the dipole's direction unit vector, which is not coincident with the Earth's rotation axis, and expressed as

$$\begin{aligned} \hat{\mathbf{N}} &= \begin{bmatrix} \hat{N}_x \\ \hat{N}_y \\ \hat{N}_z \end{bmatrix} \\ &= \begin{bmatrix} \sin\gamma\cos\beta \\ \sin\gamma\sin\beta \\ \cos\gamma \end{bmatrix} \end{aligned} \tag{3.46}$$

$$\tilde{\omega} = \begin{bmatrix} 0 & 0 & \omega_e \end{bmatrix}^T \tag{3.47}$$

with $\gamma = 10.26°$ as the angle measured between the magnetic and geocentric north pole, and $\beta = \beta_{Go} + \omega_e t$, where β_{Go} is the Greenwich's longitude and $\omega_e = 4.1667 \times 10^{-3}(°/s)$ is the Earth's angular rotation rate [36], [47].

3.7 Equations for Relative Motion

The relative motion of two arbitrary satellites in formation can be described by the linear approximation equations named after the Hill-Clohessy-Wiltshire (HCW) [39]. Taking the Hill reference frame as in, Fig. 3.6, the HCW model offers an analytic solution for the free motion of two or more satellites in an orbital system with an origin moving along the circular orbit in the central gravitational field. HCW equations offer a linear approximation for the relative orbital motion, equations that otherwise would be too complex for the analytical solution. However, this model can only be used in situations where the inter-satellite distance is much smaller than the reference orbital point radius [11]. Several assumptions are applied while solving these sets of equations, to simplify the derivation processes, hence affecting the accuracy of the results. The full process of linearization to obtain the HCW equations set can be found in Appendix A.1.

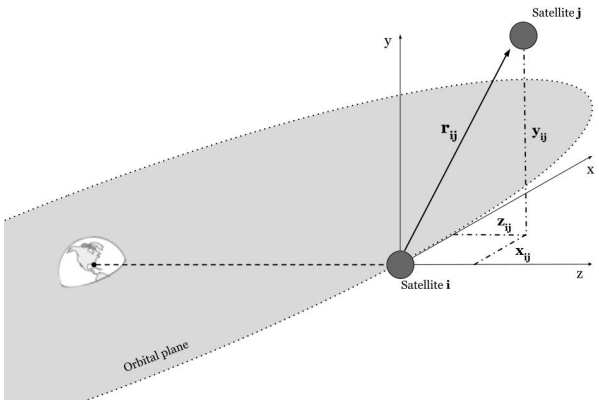

Figure 3.8: Representation of a relative motion translated by the equations.

Assuming that both the $i-th$ and $j-th$ satellite position vectors expressed in LVLH are represented by $\mathbf{r_i} = \begin{bmatrix} x_i, & y_i, & z_i \end{bmatrix}$ and $\mathbf{r_j} = \begin{bmatrix} x_j, & y_j, & z_j \end{bmatrix}$ respectively, and considering that the relative motion between them both is described by $\mathbf{r_{ij}} = \mathbf{r_j} - \mathbf{r}_i = \begin{bmatrix} x_{ij}, & y_{ij}, & z_{ij} \end{bmatrix}$, with $i = 1, \ldots, N;\ j = 1, \ldots, N$, the HCW equations are as follows

$$\ddot{x}_{ij} + 2\omega\dot{z}_{ij} = 0 \tag{3.48}$$

$$\ddot{y}_{ij} + \omega^2 y_{ij} = 0 \tag{3.49}$$

$$\ddot{z}_{ij} - 2\omega\dot{x}_{ij} - 3\omega^2 z_{ij} = 0 \tag{3.50}$$

The solution for this provided by

$$x_{ij}(t) = -3C_1^{ij}\omega t + 2C_2^{ij}\cos\omega t - 2C_3^{ij}\sin\omega t + C_4^{ij} \tag{3.51}$$

$$y_{ij}(t) = C_5^{ij}\sin\omega t + C_6^{ij}\cos\omega t \tag{3.52}$$

$$z_{ij}(t) = 2C_1^{ij} + C_2^{ij}\sin\omega t + C_3^{ij}\cos\omega t \tag{3.53}$$

where the effects of the initial conditions are represented by the constants $C_1, \ldots, C_6$, which are defined as follows

$$C_1^{ij} = \frac{\dot{x}_{ij}(0)}{\omega} + 2z_{ij}(0) \tag{3.54}$$

$$C_2^{ij} = \frac{\dot{z}_{ij}(0)}{\omega} \tag{3.55}$$

$$C_3^{ij} = -3z_{ij}(0) - \frac{2\dot{x}_{ij}(0)}{\omega} \tag{3.56}$$

$$C_4^{ij} = x_{ij}(0) - \frac{\dot{z}_{ij}(0)}{\omega} \tag{3.57}$$

$$C_5^{ij} = \frac{\dot{y}_{ij}(0)}{\omega} \tag{3.58}$$

$$C_6^{ij} = y_{ij}(0) \tag{3.59}$$

corresponding to the C constants values calculated through the velocity or the position vector components at $t = 0$, and the ω is defined as the orbital angular velocity.

From the homogeneous solution, we can also highlight the terms that are responsible for defining the relative orbit. The term responsible for the relative drift is $-3C_1{}^{ij}\omega t$, which defines the drift of the instant ellipse center in the along-track direction. This effect is ex-

perienced by a satellite relative to the reference orbital point and it is defined by the initial conditions. The drift can also be caused by environmental perturbations and nonlinear effects. To achieve a bounded multi-satellite configuration, this drift factor, C_1^{ij} (3.54), should be eliminated or, at least, the applied control should lead to practically negligible value. The size of the in-plane ellipse is defined by C_2^{ij} and C_3^{ij} terms (3.55) and (3.56), and similarly, the out-of-plane motion amplitude is defined by the C_5^{ij} and C_6^{ij} constants (3.58) and (3.59). The instant center of the ellipse displacement is represented by the C_4^{ij} term (3.57), also referred to as relative shifts in the along-track direction. This last parameter is responsible for obtaining the specific distribution of the satellites within the configuration.

Consider a new controlled motion equations set, the **u** parameters, presented below (3.60)-(3.62). The control vector **u** represents the required acceleration to correct the relative motion of the formation. The control vector has three components, u_x, u_y and u_z along the x, y and z axis respectively, which grants a more precise and sensitive control calculation.

$$\ddot{x}_{ij} + 2\omega\dot{z}_{ij} = u_x \tag{3.60}$$

$$\ddot{y}_{ij} + \omega^2 y_{ij} = u_y \tag{3.61}$$

$$\ddot{z}_{ij} - 2\omega\dot{x}_{ij} - 3\omega^2 z_{ij} = u_z \tag{3.62}$$

To simplify the calculation of the required controlled state values, the following trajectory constants are considered:

$$B_1 = C_1 \tag{3.63}$$

$$B_2 = \sqrt{C_2^2 + C_3^2} \tag{3.64}$$

$$B_3 = -3C_1\omega t + C_4 \tag{3.65}$$

$$B_4 = \sqrt{C_5^2 + C_6^2} \tag{3.66}$$

$$\sin \psi_1 = \frac{C_3}{\sqrt{C_2^2 + C_3^2}} \tag{3.67}$$

$$\sin \psi_2 = -\frac{C_6}{\sqrt{C_5^2 + C_6^2}} \tag{3.68}$$

$$\cos \psi_1 = \frac{C_2}{\sqrt{C_2^2 + C_3^2}} \tag{3.69}$$

$$\cos \psi_2 = \frac{C_5}{\sqrt{C_5^2 + C_6^2}} \tag{3.70}$$

Above, a new set of trajectory parameters are defined in (3.63-3.68). These parameters transformation allows an easier interpretation of the free satellites relative motion as is presented bellow.

After the transformation from the C parameter to the B's, the following transformations in the HCW equations are implemented

$$x(t) = 2B_2 \cos \psi_1 + B_3 \tag{3.71}$$

$$y(t) = B_4 \cos \psi_2 \tag{3.72}$$

$$z(t) = B_2 \sin \psi_1 + 2B_1 \tag{3.73}$$

Hence, resulting in a different solution representation of HCW-based equations set for relative motion discussed in this work.

From the previous solutions it is possible to conclude that B_1 is the parameter describing the instant ellipse drift, B_3 is responsible for the ellipse center shift (at the initial moment), while B_2 and B_4 describe the ellipse in-plane and out-of-plane motion amplitude, respectively.

In order to solve these equations it is therefore necessary to find the first derivatives

$$\frac{d}{dt}\left(x_{ij}\right) = -2B_2\omega\sin\psi_1 - 3B_1\omega \tag{3.74}$$

$$\frac{d}{dt}\left(y_{ij}\right) = -B_4\omega\sin\psi_2 \tag{3.75}$$

$$\frac{d}{dt}\left(z_{ij}\right) = B_2\omega\cos\psi_1 \tag{3.76}$$

With this new equations set it is therefore possible to solve the (3.71) - (3.73) and thus obtaining the HCW relative motion controlled equations. This is a critical equations set for the control system studied in this work, once all the Lyapunov-based functions and the control algorithm developed are based in these variables modifications and posterior simplifications, presented bellow

$$\dot{B}_1 = \frac{1}{\omega}u_x \tag{3.77}$$

$$\dot{B}_2 = \frac{1}{\omega}\left(u_z\cos\psi_1 - 2u_x\sin\psi_1\right) \tag{3.78}$$

$$\dot{B}_3 = -3B_1\omega - \frac{2}{\omega}u_z \tag{3.79}$$

$$\dot{B}_4 = -\frac{1}{\omega}u_y\sin\psi_2 \tag{3.80}$$

$$\dot{\psi}_1 = -\frac{1}{\omega B_2}\left(u_z\sin\psi_1 + 2u_x\cos\psi_1\right) \tag{3.81}$$

$$\dot{\psi}_2 = -\frac{1}{\omega B_4}\left(u_y\sin\psi_2\right) \tag{3.82}$$

3.8 Lorentz-force explanation

This paper aims for the development of a viable propellantless formation flying control, thus, it is necessary to describe the technical aspects of the electromagnetic force used in this paper. Any charged particle, moving with a given velocity relative to a magnetic field, accelerates. This acceleration is directed along the normal vector of the plane formed by the velocity and magnetic field vectors. This effect is called the Lorentz force [36], [47]. This force is valid for

any charge q with a relative velocity $\mathbf{v}$ in an electric and magnetic field, $\mathbf{E}$ and $\mathbf{B}$ respectively, and is given by

$$\mathbf{L_F} = q(\mathbf{E} + \mathbf{v} \times \mathbf{B}), \tag{3.83}$$

Charged spacecraft orbiting the Earth are affected by this force too, however unlike the Coulomb force effects, the Lorentz force is not resultant from the interaction between two charged satellites[36], [47]. The Lorentz force case, is caused by the interaction between the spacecraft's velocity and the Earth's rotating magnetic field. Note that both direction and magnitude of the Lorentz force depend on the satellite orbital motion. These Lorentz force vector is depicted in the Fig. 3.7.

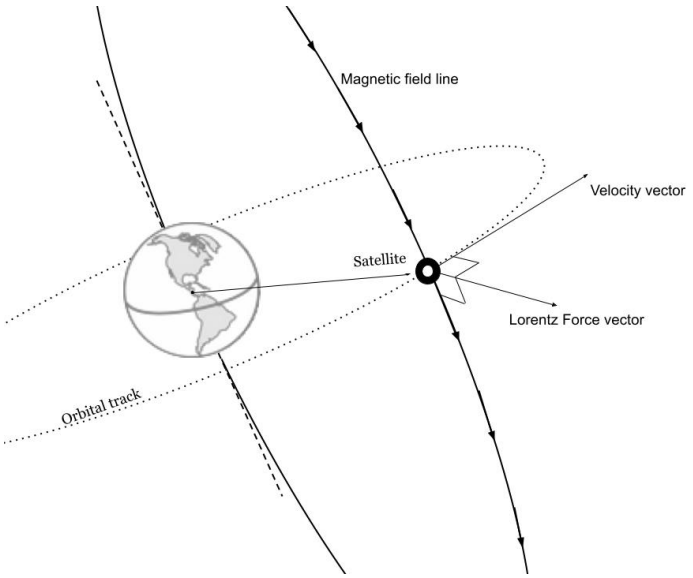

Figure 3.9: Representation of the Lorentz force effect in a orbiting body.

Another important factor is related to the Debye shielding whose effects, depending on the orbit's altitude and geometry, may influence the orbiting charged satellite. Debye shielding is a concept responsible to quantify the response of the environment (in this case the plasma surrounding) to electrical fields when releasing charged particles. This effect is quantified through the Debye length, a measure of the electrostatic net effect of a charge carrier, and how far it persists. For the LEO the measured Debye length values are small $\left(\cong 1cm\right)$, and the satellite velocities are much larger than the magnetic field rotational speed, which leads to the overlapping of the Lorentz force over other electromagnetic forces such as the Coulomb force. Therefore, the existence of Debye shielding results in a functioning improvement in Lorentz-capable spacecraft. The presence of this Debye effect enhances the charge storage capacity, hence enhancing LAO systems performance when in LEO [13]. With the rise of orbital altitude comes a Debye length increase, which combined with the lower spacecraft's relative velocity (to the magnetic field) results in the dominance of the Coulomb effects over

the Lorentz force. Thus, at LEO, satellite formation control systems requiring Coulomb's attractive and repulsive force-based devices are not as effective as the those based on the Lorentz force.

Contrasting with the propellant-based systems, LAO capable devices offer the prospect of a renewable and non-finite thrust, and therefore presenting the possibility of establishing different flying formations, from the train formation type to a nested ellipses. Since the usage of a link between the Lorentz force and the Coulomb effects reveals to be, theoretically, incompatible for LEO, it is therefore important to explicit that these formations control was developed relying on positioning control of the single spacecrafts, revealing no inter-satellite pairing system. However, through the design and development processes of an electromagnetic formation control system, for the practical real-life cases, it is necessary to consider both Coulomb and Lorentz effects on a charged satellite, even though theoretically the minor Coulomb effects while in LEO [13].

When considering LAO capable systems, there are some aspects relative to the system's morphology that should be accounted in the design phase. The first one is the maximization q/m, once the Lorentz force reveals to be proportional to the charge. However, the charge losses rate to the environment should be a major concern, once this rate will be directly linked to the power required for the control system functioning, thus the design's discharge susceptibility shall be closely examined. From studies such as [30] and [13], the best achieved design for a LAO spacecraft is with a surface of a conducting sphere, though this shape preludes charge concentrations that would otherwise encourage arcing and discharge into the plasma. To counter this phenomena, the authors propose the action of designing a surrounding conducting sphere, therefore establishing a Faraday cage that would completely protect the interior components from electrical discharge.

Although the present work does not focus on the design study of LAO equipment's, but rather in the study and validation of such technology, the previous paragraph was written as an overview of the possible designs of these systems.

Chapter 4

Control Algorithm Development

A control algorithm is a set of logically programmed stages that can perform a task/action autonomously based on the environmental measured values. In space missions, this is one of the most important characteristics of the system, since small automatic corrections are needed to be performed constantly to perform the mission. These corrections would not otherwise be possible without this type of autonomous algorithm. Particularly in formation flying missions, the control algorithms play a vital role, once it is responsible to continuously check for the system elements motion, and even for their attitude in some cases. This chapter is dedicated to giving a review on the basis that enabled the development of the control algorithm for this study.

4.1 Problem Statement

After clarifying the models and dynamics employed as a ground basis for this work, this section resumes the assumptions and correlations assumed while formulating the formation flying control objective.

Bearing in mind all the aspects related to the satellite formation flying problem, this work focuses on the development of a relative motion control algorithm for a multiple satellite configuration solely using the Lorentz force. Therefore, this work aims to test and verify the developed algorithm for a group of satellites to achieve the required relative motion through the interaction between an onboard charging component and the external magnetic field generated by Earth. Hence, the final objective is to study the performance of relative motion control using the Lorentz force.

The problem statement of this work is as follows. Several satellites equipped with charging capable devices are considered to be in LEO. The Earth magnetic field is modelled as the tilted dipole model previously described in Chapter 3. The satellites are considered to be point masses, whose attitude motion is not considered throughout the work. Due to the influence of the Debye shielding in LEO orbits, inter-satellite and Earth-satellite electrostatic interaction is neglected. For simulation of controlled motion, the second harmonic of the geopotential J_2 is taken into account as the only environmental perturbation. Once the satellites are considered to be point masses equipped with charging capable devices, there is no full controllability of the translational relative motion. Thus, the objectives of the control algorithm are to eliminate the formation relative drift, to achieve the required value for the relative shift as well as out-of-plane and in-plane relative trajectory amplitudes. The phase

angles for the in-plane and out-of.plane relative motion remain uncontrolled. To achieve this goal, a Lyapunov-based control algorithm is developed.

It is also necessary to study the performance of the developed algorithm depending on a large variety of factors, such as charging capacity maximum value, orbital height, and the variation of the initial conditions. The Monte-Carlo simulations method is used to evaluate the influence of these parameters on the convergence time or the accuracy of the control algorithm.

4.2 Lyapunov-based control

The proposed control algorithm goal is to control and maintain a satellite formation after the orbital deployment. The direct Lyapunov method is applied for the development of the control algorithm. This method provides the stability of a body's controlled motion [48].

Building the Lyapunov functions for a given automatic control system enables the estimation of the time and quality variation of the control. This method begins by defining an attraction region and, consequently, develops a state for the initial values. By giving a prevision of the area of the initial disturbance (which, over time, is not exceeded), this method provides a solution for the over-correction problem [48].

In order to reach this stability state, it is necessary to satisfy the following theorems [49], [50]:

1. *Theorem: If for the differential equations of a perturbed motion we can find a definite function V such that by virtue of the given equations its derivative $\dot{V}$ is either identically equal to zero or is semidefinite with the opposite sign of V, then the unperturbed motion is stable.*

2. *Theorem: If one can find a definite function V for the differential equations of a perturbed motion such that its first derivative $\dot{V}$ is also a definite function but with the opposite sign of V, then the unperturbed motion is asymptotically stable.*

3. *Theorem: If for differential equations of the perturbed motion one can find a positive definite function $V(x)$ such that*

$$\lim_{x \to +\infty} V(x) = \infty \tag{4.1}$$

and its derivative evaluated by the virtue of the differential equations satisfies the following two conditions for all x:

(a) $\dot{V} < 0$, outside K.

(b) $\dot{V} = 0$*, inside* K*.*

where K *is the manifold of the points not containing whole trajectories of the system for* $0 \leq t < \infty$*, then the unperturbed motion* $x = 0$ *is stable in the large. (The notation* $x \to \infty$ *in the equation (4.1) means that at least one coordinate* x_k *converges to infinity via any path) .*

These theorems are used for the control function development. Thus, since the purpose of the control algorithm is to achieve the required B_i, $i = 1, 2, 3, 4$ parameters, the following parameters deviations are considered

$$\begin{aligned} \Delta B_2 &= B_{2inst} - B_{2des}, \\ \Delta B_3 &= B_{3inst} - B_{3des}, \\ \Delta B_4 &= B_{4inst} - B_{4des}, \end{aligned} \tag{4.2}$$

where the relative orbit ellipse is defined by the B_{ides} elements, with the *des* index defining the desired parameters, and the B_{inst} representing the instantaneous parameter values measured along the orbit track. The implementation purpose of these equations is to allow the formation to maintain the required relative orbit shape. Important to remark that being the main goal of the present work the elimination of the drift, the difference between the instantaneous B_1 and the desired was not considered once it would result in a extra redundant step.

The relative orbit control is divided into two stages: a first one with the objective of eliminating the drift and achieving the desired ellipse shift; and then a second one where the desired in-plane and out-of-plane motion amplitudes are obtained.

In order to set the relative drift B_1 and the relative shift ΔB_3 to zero, the following Lyapunov function was developed for the first stage:

$$V = \frac{1}{2}B_1^2 + \frac{1}{2}\Delta B_3^2, \tag{4.3}$$

where the B parameters come after the defined in (3.60) to (3.65). Deriving the equation above with time, and substituting some of the terms for the simplifications presented in (3.78) to (3.83)

$$\begin{aligned}\dot{V} &= B_1\dot{B}_1 + \Delta B_3\Delta\dot{B}_3, \\ &= \frac{1}{\omega}B_1 u_x + \Delta B_3\left(-3B_1\omega - \frac{2}{\omega}u_z\right),\end{aligned} \tag{4.4}$$

where the $\dot{B}_i$, $i = 1, 2, 3, 4$ represent the first time derivatives of the B_i parameters, described in the previous chapter. Thus, in order to achieve $\dot{V} < 0$ and obtain the global asymptotic stability, when $B_1 = 0$ and $\Delta B_3 = 0$, is the following control should be applied

$$u_x = -k_a B_1, \quad k_a > 0 \tag{4.5}$$

$$u_z = \frac{1}{2}(-3B_1\omega^2 + k_2\omega\Delta B_3), \quad k_b > 0 \tag{4.6}$$

After reaching the desired values for B_1 and B_3, inside the convergence zone, the algorithm starts a second stage, in order to achieve both the in-plane and out-of-plane required trajectory amplitude values. Thus, the following Lyapunov function used is

$$V = \frac{1}{2}B_1^2 + \frac{1}{2}\Delta B_2^2 + \frac{1}{2}\Delta B_3^2 \tag{4.7}$$

its time derivative is the following

$$\dot{V} = -\frac{1}{\omega}\left(B_1 - 2\Delta B_2\sin\psi_1\right)u_x + \frac{1}{\omega}\left(\Delta B_2\cos\psi_1 - 2\Delta B_3\right)u_z - 3B_1\Delta B_3\omega \tag{4.8}$$

from which the following control is derived

$$u_x = -k_x\left(B_1 - 2\Delta B_2\sin\psi_1\right), \; k_x > 0 \tag{4.9}$$

$$u_z = -k_z\left(\Delta B_2\cos\psi_1 - 2\Delta B_3\right), \; k_z > 0 \tag{4.10}$$

which results in

$$\dot{V} = -\frac{1}{\omega}\left(B_1 - 2\Delta B_2 \sin\psi_1\right)^2 - \frac{1}{\omega}\left(\Delta B_2 \cos\psi_1 - 2\Delta B_3\right)^2 - 3B_1\Delta B_3\omega \tag{4.11}$$

the term $-3B_1\Delta B_3\omega$ could not be negative, but after the first control stages its value will be much smaller than the sum of the first and second terms in this equation. Therefore, it is assumed that this term takes a rather insignificant impact on the Lyapunov function derivative.

It should be noted that the calculated control according to the eq.(4.5, 4.6, 4.9 and 4.10) may not be possible to implement considering the system's charging capacity limits. Henceforth,it is required to take into account the implementation restrictions during the controlled motion simulation. This important issue is addressed in the next section.

Inside the second stage the control of the out-of-plane trajectory amplitude is also implemented. It is obtained using the following Lyapunov function

$$V = \frac{1}{2}\Delta B_4^2 \tag{4.12}$$

with the corresponding time derivative as

$$\dot{V} = \Delta B_4 \Delta \dot{B}_4 \tag{4.13}$$

form which the control is as follows

$$u_y = -k_y \Delta B_4 \sin\psi_2, \quad k_y > 0 \tag{4.14}$$

thus, controlling the size of the relative trajectories along the vertical y-axis.

Throughout the explanation of the resultant control relations, it is possible to denote the presence of a k parameters in the functions. The key role of this k parameter is associated with the Lyapunov control convergence velocity. It always represents a positive number, whose value and magnitude may vary depending on the available control source.

The Lyapunov controls described above are developed without any restrictions concerning the control system. It is then necessary to consider the possible implementation issues when using the Lorentz force.

4.3 Control implementation using Lorentz-force

As referred to in the previous paragraph, it is now necessary to implement the calculated control. The description of the system morphology that enables the Lorentz force utilization is described in section 3.8 of chapter 3. In this section, the main features of the Lorentz force are taken into account to implement calculated control.

Important to recall that the control force is produced as the result of the direct interaction between Earth's magnetosphere and the satellites charged point of mass. The first step is to calculate the magnetic field vector for the current position of the satellite, according to the equation that is responsible to calculate the Lorentz force, Eq.(3.69), and the satellite velocity vector. Since the Lorentz force direction vector is defined and the control source is the charge of the satellite (a scalar value), it is now possible to implement the calculated control vector $\mathbf{u_i}$ at each time step. In order to implement each component of the calculated control, three different values of the satellite charge should be implemented

$$q_x = \frac{u_x}{L_x} \tag{4.15}$$

$$q_y = \frac{u_y}{L_y} \tag{4.16}$$

$$q_z = \frac{u_z}{L_z} \tag{4.17}$$

where $[u_x, u_y, u_z]$ are the control components (4.5),(4.6),(4.9),(4.10) and (4.14) enumerated in the previous chapter, and $[L_x, L_y, L_z]$ are the Lorentz force vector components along the three reference frame axis. However, the charge of the satellite is a scalar value so there cannot be three distinct charges being applied simultaneously. Thus, the calculated control vector cannot be implemented as it is. So, to calculate the single charging value that is going to be applied it is required to calculate a Lorentz force value that is close to joint magnitude of the three calculated control vectors.

In order to implement this idea, the following single charge calculation is proposed

$$q_{mean} = \sqrt{\frac{q_x^2 + q_y^2 + q_z^2}{3}}\ sign(q_x + q_y + q_z) \tag{4.18}$$

In this equation a critical step is taken. After obtaining the three values for the required charges (measured along the axis dictated by the Hill reference frame), the main charging

value is calculated. This value, q_{mean}, is calculated as the magnitude of the required force and its direction is defined by the strongest component, or components (through the $sign$ function).

As referred to above in this section, during the calculation of the real charging value, the system's charge limitations shall be accounted for. Thus, consider the device's maximum charge value, that can be produced by the charging device, to be q_{max}. Then whenever the calculated control exceeds the value of q_{max} the following step is activated

$$q_{mean} = \begin{cases} q_{max}\ sign(q_{mean}), & |q_{mean}| > q_{max} \\ \\ q_{mean}, & |q_{mean}| \leq q_{max} \end{cases} \tag{4.19}$$

This formula represents a stage in the control algorithm, which is only activated when the virtual charge value exceeds the limit.

So, the implemented vector of the current Lorentz force acting on the satellite charge is calculated using the following formula

$$\mathbf{L_{local}} = \left(\left(\frac{q_{mean}}{m} \right) \mathbf{v_{relative}} \right) \times \mathbf{B} \tag{4.20}$$

thus, this chapter defines the general control algorithm that is used for the relative motion control. Though the control strategies could depend on the number of satellites and on the satellites relations. These aspects are covered in the next section.

Also the limited charging rate is taken into account in the simulation process. So, while the charging device polarity altercation, the charge cannot vary more than d_{charge}, during the time interval corresponding to $t_n - t_{n-1}$. The following formula is representative of the current value q_{mean} at the time step t_n,

$$q_{mean(n)} = q_{mean(n-1)} + d_{charge}\ sign\left(q_{mean(n)} - q_{mean(n-1)}\right) \tag{4.21}$$

when,

$$|q_{mean(n)} - q_{mean(n-1)}| > d_{charge}$$

The utilization of such a step is due to the fact that in reality the polar charge changing, i.e., the charge sign (or magnitude) altercation is not an instantaneous process. Therefore this step induces a smoother transition between charging polarization's, providing closer to reality simulation results.

4.4 Decentralized control approach

When talking about the construction of a satellite formation flying and the respective algorithm development steps, it is important to choose not only the most beneficial system configuration but also an advantageous formation controlling strategy.

The definition of the control strategy nature will dictates the overall formation management of the elements relative position, a formation flying characteristic that is dependent from the chosen scheme's autonomy. Considering this dissertation proposes of using the Lorentz force as a control method, and recalling that the magnitude of this control force is dependent on either the velocity and position of the body, the control algorithm development was then based on the decentralized strategy. As previously referred, this strategy, by enabling every unit in the formation with the capability of freely managing its relative position, provides a more precise position control and a low risk of mission failure.

Taking the decentralized scheme, the following three distinct formation configuration cases were developed in order to fully understand the viability and possible usages of this technology, where the influence of the number of charging capable devices and the total number of elements in the formation are studied.

The first case assumes a configuration with an Uncharged leader and a Charged follower, where, assuming the position maintenance approach of the leader/follower method, the relative state of the follower spacecraft is controlled through the autonomous charging device and therefore correcting its motion accordingly to the position of a charging device absent leader spacecraft prescribing a previously defined parameter constant orbit. This first hypothesis corresponds to the simplest formation flying scheme and tests out the possibility of using this electromagnetic effect as a reliable control, especially in the drift elimination and the ellipse center shift mitigation.

As for the second rehearsal, a formation scheme accounting for a Virtual leader and two

Charged followers was considered, a hypothesis that considers a system where two charging capable devices individually correct their relative positioning to a virtual center, a dummy point inserted in the desired orbit to be performed. Funded on an altered leader/follower method, this proposition objective is to evaluate the performance influence of having two dynamic-charging satellites either in the global structure maintenance, as to check if the convergence, assuming its existence, is directly influenced by this condition changes.

The third case conceptualizes a formation structure based on symbiosis linking the swarm and the leader/follower approaches, in such a way that a large number of charging capable satellites individually monitor and automatically correct their relative state according to a fictional point located in the desired orbit track, assembling some characteristics of the previously described case. Taking a total number of ten elements, this case goal is the assessment of the considered control actuator for large complex structures management, namely the influence that a large elements number may have on the formation drift and shift elimination, and to evaluate the controller quality for collision avoidance situations. Once the relative positioning of the crafts is decentralized, and therefore completely independent from the vicinity elements, it is primordial to implement a secondary algorithm with the superimposing capacity of correcting and avoiding what would otherwise be a collision course. Therefore, the following equations were implemented in this third study case,

$$L_F = \begin{cases} -L_F, & |r| \leq d_{min} \\ \\ L_F, & |r| > d_{min} \end{cases} \tag{4.22}$$

where by changing the previous satellite charging value the direction of the movement is altered consequently avoiding the spacecrafts crash, when inside the danger radius neighboring area delimited by d_{min} which represents the minimum distance for this control to be effective.

To summarize the cases detail, the following scheme was developed,

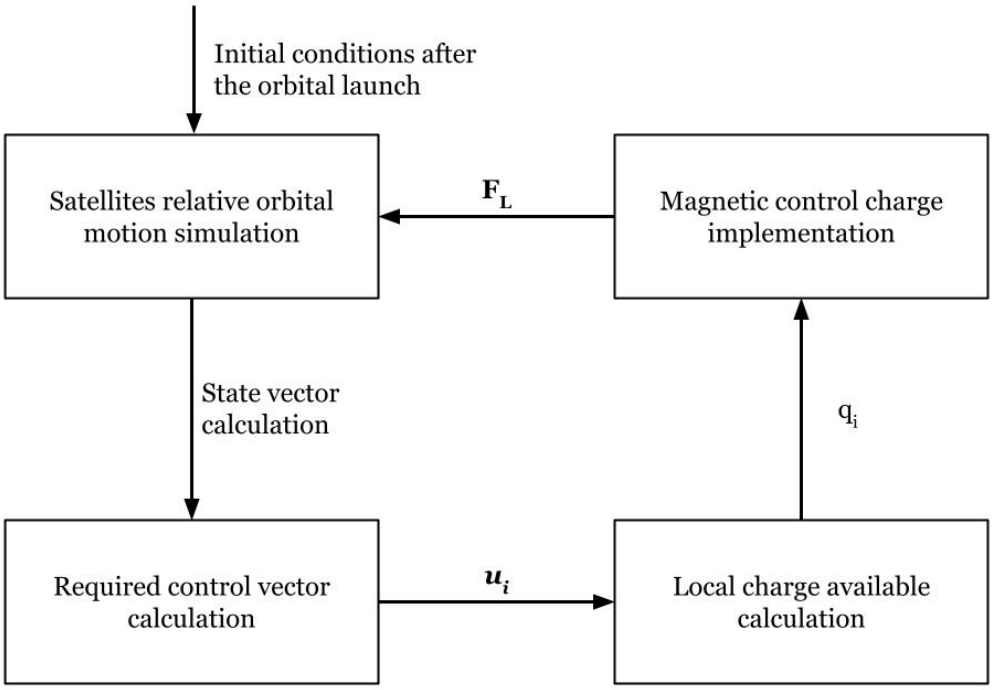

Figure 4.1: Summary of the steps taken during the control.

Chapter 5

Simulation Results

To validate the developed control algorithm based on the usage of the Lorentz force, it is necessary to test it on a set of different formation flying cases. Therefore three types of formation flying configurations are considered in the study, evaluating the performance of the proposed control for each formation type.

This chapter describes the overall implementation conditions (from the orbital environment to the control strategy or number of satellites in the formation) and lastly to present the results obtained in the numerical simulations, using different formation control approaches.

5.1 Simulation parameters description

For the base assumption, consider that all the cases of formation flying missions are at Low Earth Orbit, LEO. This section gives a scope of the conditions and parameters that make an influence on the relative motion of the formation and its control. Table 3 presents a set of different values that are used in the formation control cases studied, from the launching initial conditions, the capabilities of the onboard charging device, required relative trajectory, orbital height, and inclination.

Initial conditions	
Initial relative drift, C_1	rand([−0.5;0.5]) m
Initial relative position constants, $C_2 - C_6$	rand([5;5]) m
Satellite parameters	
Mass of the satellites, m	1 kg
Maximum charge, q_{max}	10 μC
Orbital parameters	
Orbit altitude, h	500 km
Orbit inclination, i	51.7°
Algorithms parameters	
Control gains, k_a, k_b	$10^{-6}, 10^{-4}$
Control gains, k_x, k_y, k_z	$10^{-6}, 10^{-8}, 10^{-7}$
Maximal charge change rate, dq/dt	10^{-7} C/s
Required relative orbit parameters, $B_1 - B_4$	[0, 10, 10, 10] m
Second stage algorithm threshold for B_1 and B_3	0.05m, 2.5m

Table 5.1: Simulation parameters description.

The parameters presented above were chosen to obtain the best performance of the algorithm considering the formation convergence and to reduce the relative motion constants errors.

5.2 Free motion of two satellites

This orbital motion case serves as an introductory situation to explain the formation relative drift and the consequent need for eliminating it. Therefore, a two satellites formation with random initial conditions after deployment is defined. No control is applied to the satellites so that the natural influence of the environmental conditions in an unbounded orbital relative motion is depicted. The resulting relative trajectory after the simulation is presented in Figure 5.1. Due to the launcher deployment errors, a non-zero relative drift value arises, resulting in a two-satellite formation flying apart and not achieving the desired closed motion. It may be concluded that without control, obtaining a close relative trajectory is not possible. Even in a scenario where the initial relative drift is set to zero, the environmental perturbations lead to a gradual drift increase, apart from other formation undesirable effects.

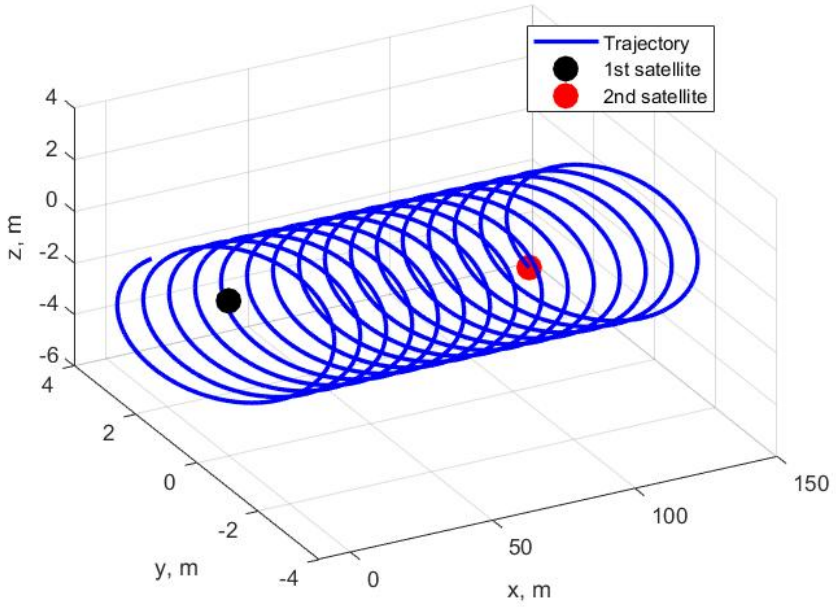

Figure 5.1: Relative trajectories free motion.

5.3 One controlled satellite study case

For the first formation simulation case, a two satellites formation is studied. Consider the application of the proposed control algorithm, described in Chapter 4, where the same initial conditions and constraints implemented in the free motion example are applied. For this case a leader-follower control strategy is studied, where the first satellite is considered to passively move along a near-circular orbit (the Leader), while the second one (the Follower) controls its relative positioning to the leader using the proposed control algorithm based on Lorenz force. The time of the controlled motion simulation is 5 days. Figure 5.2 presents an example of the relative motion.

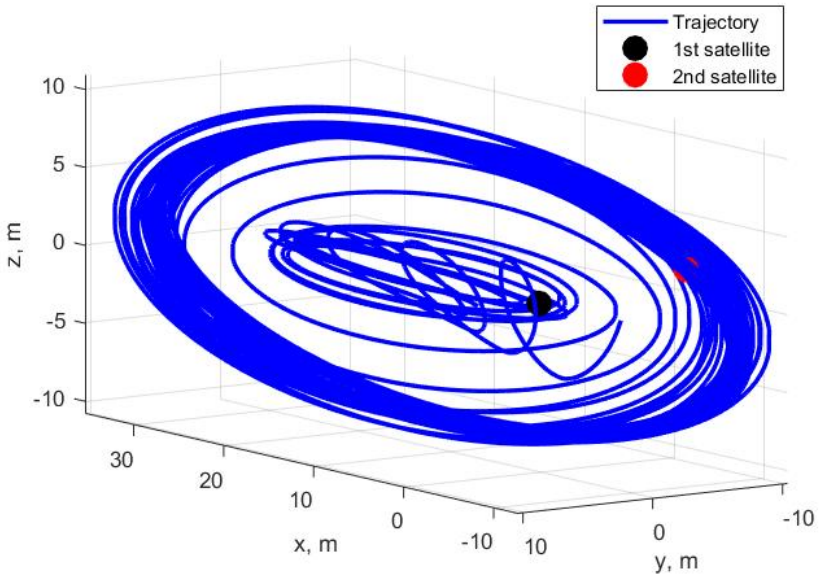

Figure 5.2: Relative trajectory under control.

It can be seen that there was an initial drift that was stopped during the first stage of the control algorithm. When the relative drift and relative shift parameters, B_1 and B_3 respectively, entered the vicinity of the required values, the second stage begun and started to change the trajectory amplitudes for the in-plane and out-of-plane motion. Fig.5.3 and 5.4 show the progression of the B constants of the controlled motion along with the required value to be achieved.

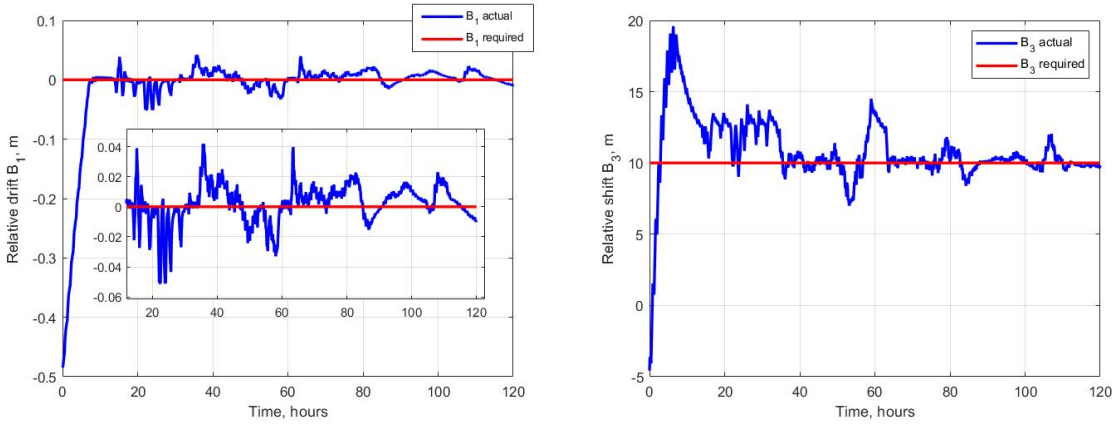

(a) Relative Drift (b) Relative Shift

Figure 5.3: The relative drift and relative shift results

From the plots, it can be concluded that the first algorithm stage took about 15 hours, the time needed for the relative shift and relative drift to reach the required values. The second stage was also about 15 hours long, during which the trajectory amplitudes got to the vicinity

of the expected values. Therefore, 30 hours after the simulation beginning, the trajectory is considered to be fully converged and with the desired shape and size achieved. The control errors caused by the control approach constraints, which are dictated by the magnitude and direction of the Lorenz force, result in trajectory parameter errors during the station keeping of the desired flying formation. The maximum deviation of the relative drift is about $0.05m$, and for the relative shift, it is about $3m$. The errors in the motion amplitudes B_2 and B_4 are smaller than or close to $1m$, hence being considered acceptable results. The implemented

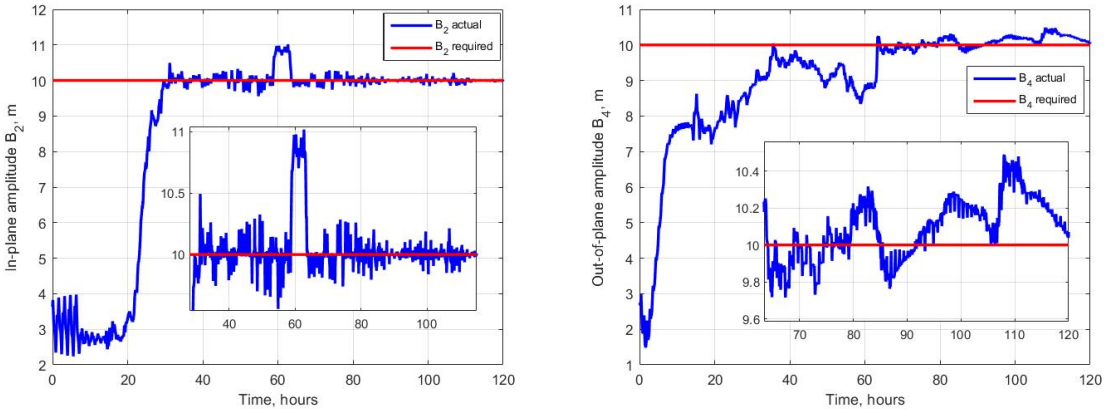

(a) In-plane motion amplitude.

(b) Out-of-plane motion amplitude.

Figure 5.4: The in-plane and out-of-plane motion amplitudes

charging values on the follower satellite during the relative motion controlling actions is presented in Fig. 5.5. It can be seen that the value of the charge is limited and its maximum is defined as 10 μC.

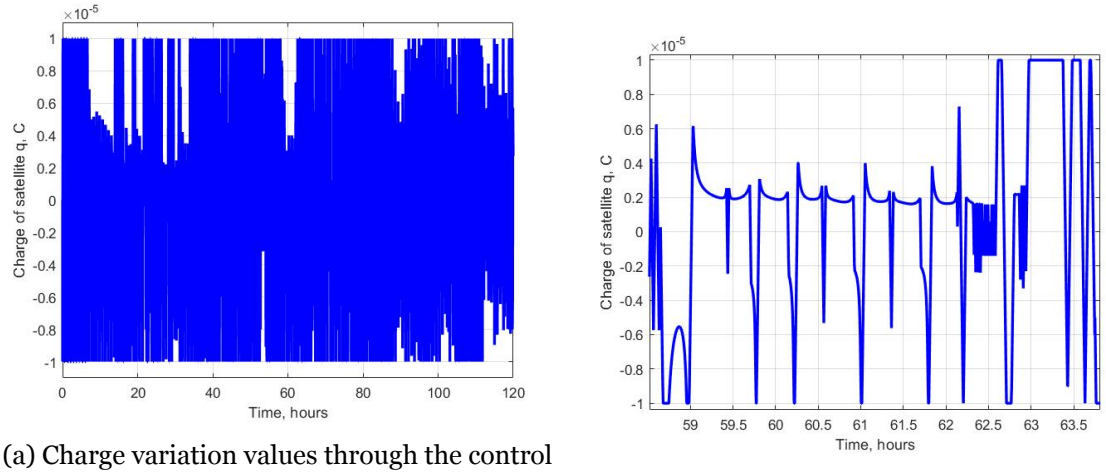

(a) Charge variation values through the control action period.

(b) Satellite charge variation (zoomed).

Figure 5.5: Charging signal variation and charging variation filter application

In the zoomed section, Fig. 5.5b, the continuous change in the charge is demonstrated. The speed of charging is also limited. Even if the required charging value suddenly changes its sign, i.e. its electric polarity, it takes time for the onboard charging system to change from its present state to the required value. In such a way the delays in the system are simulated and the limitation of the charging devices are taken into account, as was previously referred to and explained in section 4.3, Eq.(4.21), in the Control Algorithm Development chapter.

The calculated values for the control function accordingly to the Lyapunov-based algorithm are presented in Fig. 5.6.

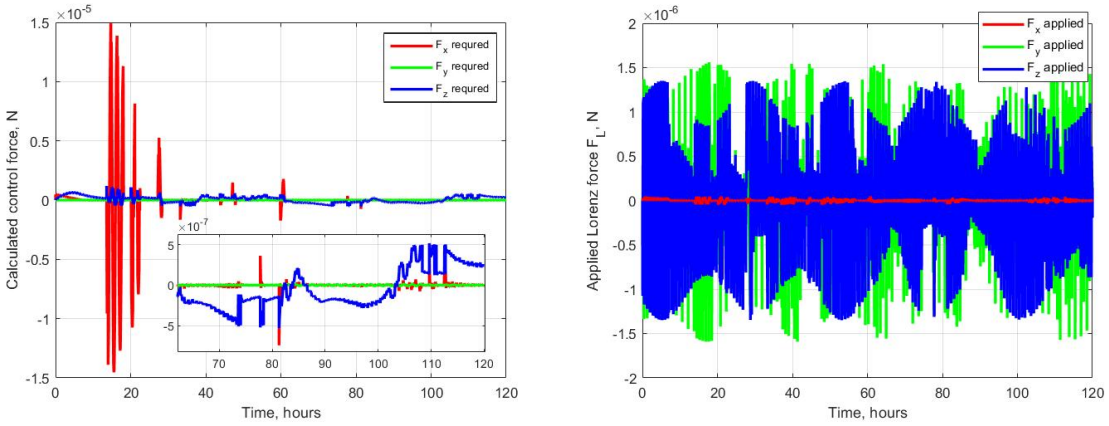

(a) Calculated control values.

(b) Applied Lorentz Force values.

Figure 5.6: Required control forces and Lorentz forces applied

The abrupt increase of the values for the required control along the x-direction is caused by the transition between the algorithm stages, from the first to the second – the deviation of the out-of-plane amplitude, B_4, was quite large and it required a longer time with the control activated. However, from figure b it is possible to verify that the real implemented values for the Lorentz force differ significantly from the calculated ones. The major divergence between the calculated and the implemented values happens for the Lorentz force component calculated for the along-track direction, being this value smaller than the other components by one order. Despite this order of magnitude difference, the relative drift is successfully mitigated while the relative shift converges to the desired value, therefore meeting the needed requirements. Since the only active control component in this study is the charge polarity and the respective variation, there are a whole set of errors associated with the implementation that are inevitable. Once the Lorenz force direction is determined by the velocity vector and local magnetic field vector, and knowing that the magnitude of the implemented control value is highly dependent on the magnitude of the most significant component (F_x, F_y or F_z). This implementation process results in a large variation error when considering the other two minor components. However, the rotation of the magnetic field vector relative to the Hill frame throughout the orbit results in a averaging upon the implementation errors and results in a trajectory convergence to the required values. From Figure 6.10 one can also

note a sinusoidal-like behavior on the peaks of Lorentz forces with a corresponding period of about 24 hours. It can be explained by the rotational motion of the tilted Earth magnetic dipole that causes a slight change in the possible direction of the Lorentz force.

The performance of the control algorithm is strongly dependent on a set of parameters, including the initial conditions. As so, by using Monte-Carlo method for the simulation process, taking randomly generated values for the initial conditions as described in Table 5.1, the elapsed time until the convergence of the B constants and the errors of the obtained trajectory parameters are studied. The analysis of the control algorithm and the subsequent data obtained by the simulations reveals that time convergence is highly influenced by the initial relative drift B_1 value. This time of convergence is defined in the instant when all the B parameters are inside the previously defined range of the required values. Concerning the simulations, for each randomly generated value for the initial relative drift where performed a total of 50 trials in order to properly evaluate the influence of this effect and to ensure the simulation results. In Fig. 5.7 the results box-plots obtained for these simulations are represented.

Inside the box are 50% of the simulations results, below and under the box are 25%, the red line is a mean value. One can see that the more the initial drift, the larger the convergence time.

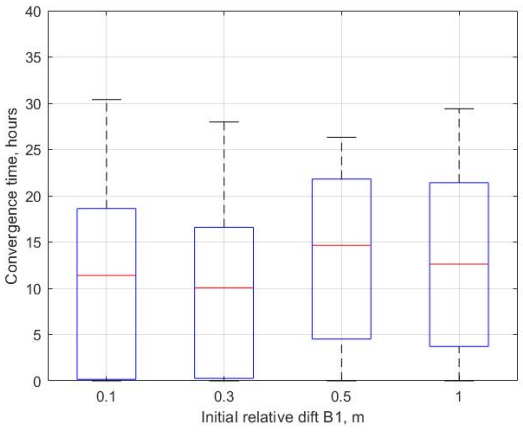

Figure 5.7: Time convergence vs Initial Drift

Fig. 5.8 and 5.9 demonstrate the errors in the B parameters of the trajectory after the time convergence. From these results, it can be concluded that there is no sensible dependence of these errors on the initial relative drift value.

Relative drift errors are inside the $2m$ range, while for B_2 this range is about $0.5m$, being the B_4 (corresponding to the out-of-plane amplitudes) the only parameter presenting a error sensitivity of several meters.

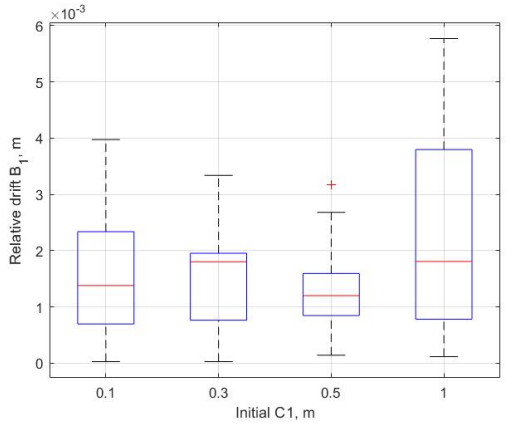

(a) Mean error in B_1 after the convergence.

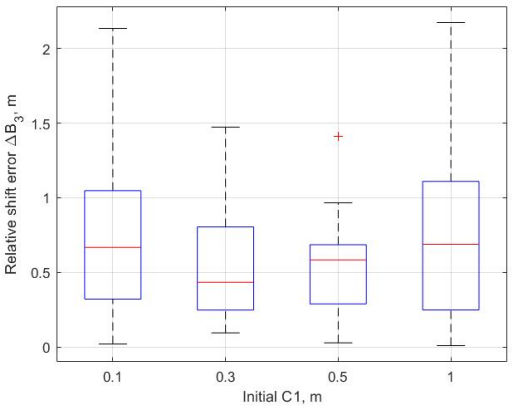

(b) Mean error in B_3 after the convergence.

Figure 5.8: Relative Drift and Shift Mean errors boxplots

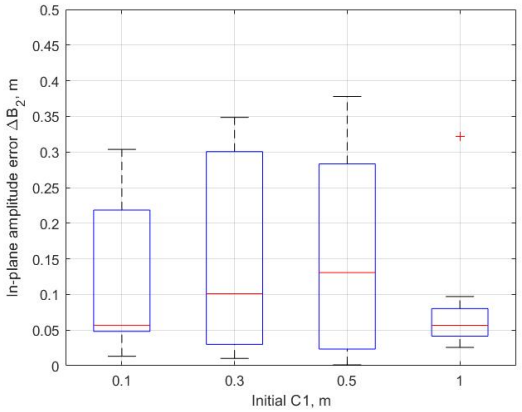

(a) Mean error in B_2 parameter after the convergence.

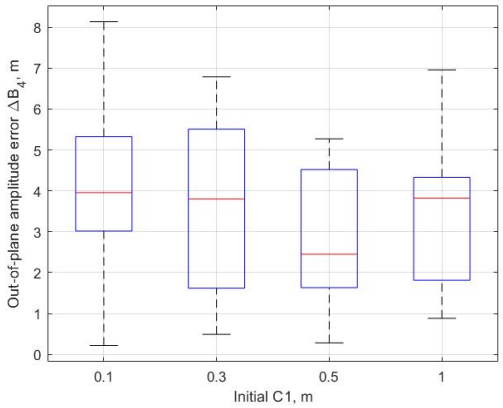

(b) Mean error in B_4 parameter after the convergence.

Figure 5.9: In-plane and Out-of-plane motion amplitude ranges Mean errors boxplots

Besides being sensitive to initial relative drift, the algorithm also shows a dependence on the maximum charge value possible for the onboard charging device. Therefore, Monte-Carlo simulations for different maximum charge values were also carried out. The time convergence box-plot is presented in Fig. 5.10, where it is possible to verify that the convergence time reduces significantly as the values for the maximum charge q became larger. This behavior can be explained by the fact that an increasing implemented control force value results in a faster approach to the required trajectory. According to Fig. 5.10, simulating a relative orbital motion from some random initial conditions, there are some isolated cases where the convergence could take a considerable amount of time (up to 30 hours) even for the maximum charge value of q. Despite these rare cases, for most of the Monte-Carlo simulations, the mean value results show that the average time convergence is about 2 hours for the considered example.

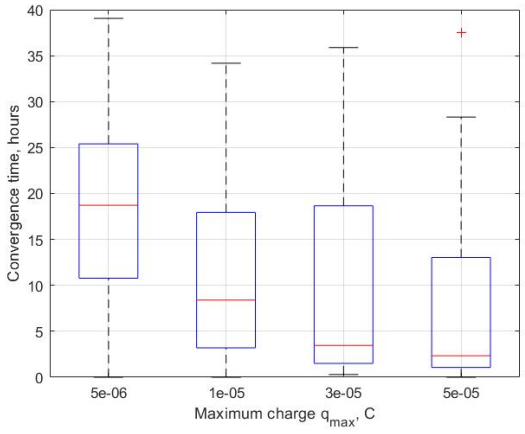

Figure 5.10: Time convergence vs Maximum charge

The results after the convergence reveal to be quite interesting, once both the relative drift, B_1, and relative shift, B_3, errors seem to take no influence with the rise of the maximum charge q value, as presented in Fig. 5.11. On the contrary, for the in-plane and out-of-plane amplitude errors, B_2 and B_4, the maximum charge increase reveal a strong dependence of these parameters on the charging value. A high q_{max} value corresponds to a greater mean value of the error and its variance.

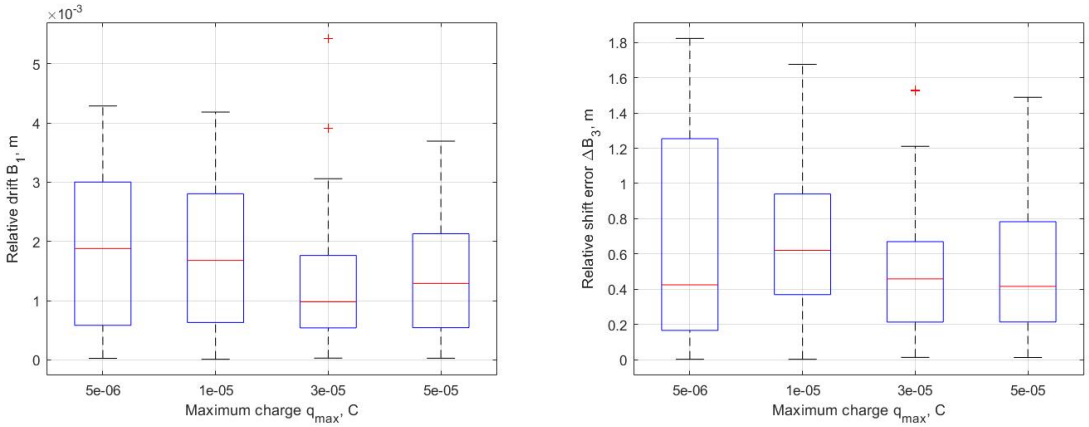

(a) Mean error in B_1 after the convergence.

(b) Mean error in B_3 after the convergence.

Figure 5.11: Relative Drift and Shift Mean error boxplots after q_{max} variation

From the Fig. 5.12 it is possible to realize that in some cases the amplitudes registered are not acceptable considering the goal values, as for the B_2 the mean error exceeds the $10m$ and for B_4, despite smaller, the mean error surpasses the $5m$ mark. This error effect is explained by the associated errors inherent to the previously described effects of using the Lorentz force as a control method, as the required control vector, either its direction and value are implemented only partially due to constraints of the Lorenz force. Such an implementation inevitably leads to disturbances caused by control errors. Therefore, the larger the q values,

the higher the level of these disturbances. From Fig. 5.12 it can be concluded that the effect of this enlarging disturbance is only witnessed in B_2 and B_4 constants increasing the value of the error.

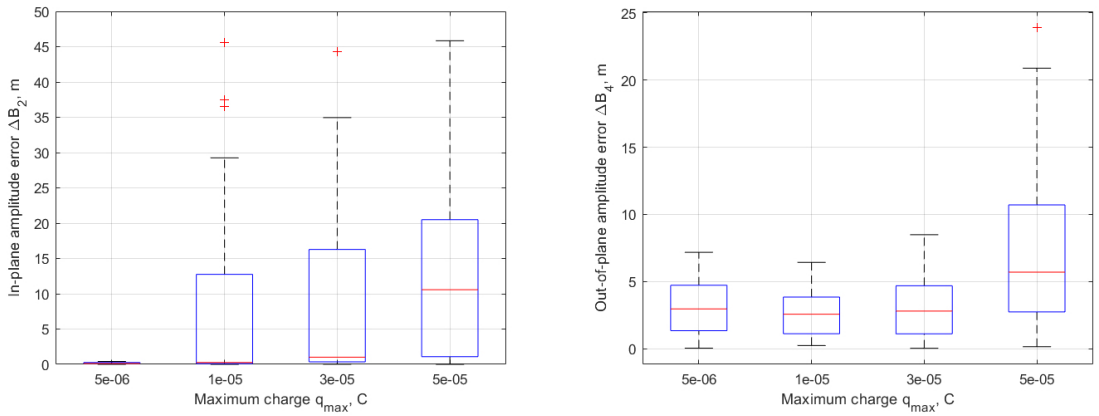

(a) Mean error in B_2 after the convergence.

(b) Mean error in B_4 after the convergence.

Figure 5.12: In-plane and Out-of-plane motion amplitude ranges Mean error boxplots after maximum charge value variation

Since the control is based on the Lorenz force, which is an effect resulting from the cross product of the local magnetic field and the satellite's velocity, the control ability depends on a magnetic field direction changing in the inertial reference frame along the orbit. However, if the satellite is placed in an equatorial orbit, the geomagnetic field vector direction is almost constant throughout the orbital motion. Also, if the satellite has a polar orbit placement, the geomagnetic field vector has components only in the orbital plane. These constraints on the geomagnetic field vector direction cause a great influence on the control algorithm performance. Thus, another Monte-Carlo simulation set was performed, accounting for the fixed random generation of the initial parameters presented in 5.1 and different values for the orbit plane inclination.

As expected, for an equatorial orbit, the proposed Lorenz force control is not working as presented in the simulation results. It is caused by an almost constant direction of the geomagnetic field vector along the orbit that results in a fixed direction of the Lorenz force. The control algorithm starts converging to the required trajectory at orbital plane inclinations from about 30°. Fig. 5.13 presents the time convergence results from the Monte-Carlo simulations for three different inclination values: 30°, 51.7° and 90°. From the graphics it is possible to denote that orbits with polar inclinations registered a lower time convergence, reason that can be explained by the rotating geomagnetic field vector direction along the orbital path, thus offering wider directional control options for the force.

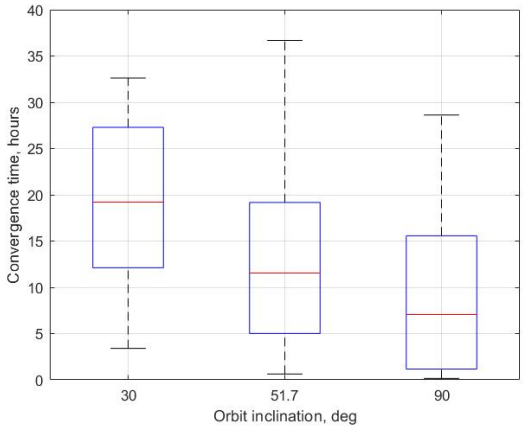

Figure 5.13: Formation convergence time depending on the orbital relative inclination variation.

Fig. 5.14 present the results from Monte-Carlo simulations for inclination variation as the errors in the trajectory parameters after convergence. Concerning the relative drift error, B_1, it is not affected by the orbital inclination, maintaining the same distance error values after the convergence through the three different trials. Relatively to the B_3, relative shift, error it is shows an error improvement with the rise of the orbital inclination, reaching an error of about 0.25 meters for a polar orbit.

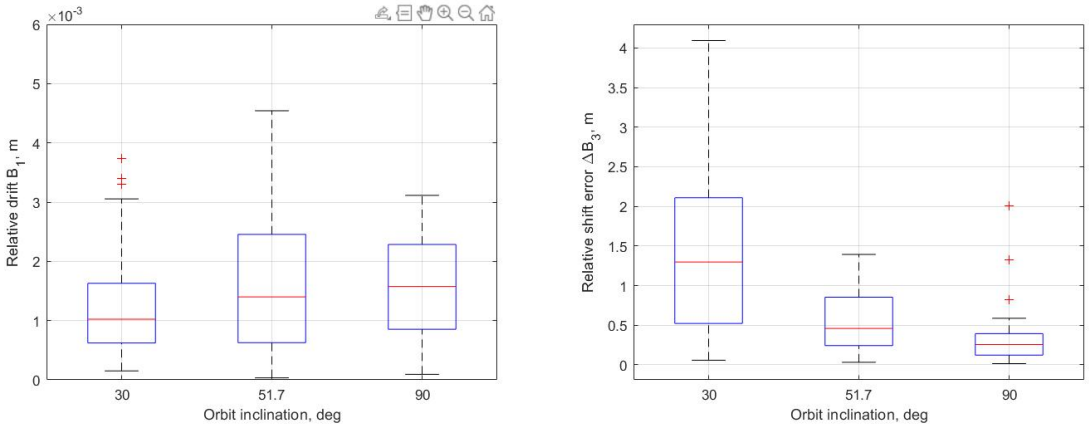

(a) Mean error in B_1 after the convergence.

(b) Mean error in B_3 after the convergence.

Figure 5.14: Relative drift and shift mean errors when subjected to different orbital plane inclination values

The same behavior is registered for the in-plane amplitude error which decreases dramatically with rising of the inclination value, Fig. 5.15. On the other hand, the out-of-plane amplitude are influenced in an almost opposite way, despite the error values not exceeding the 10 meters for the worst cases.

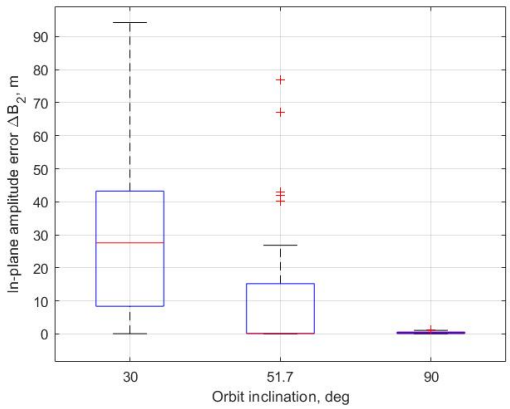

(a) Mean error in B_2 after the convergence.

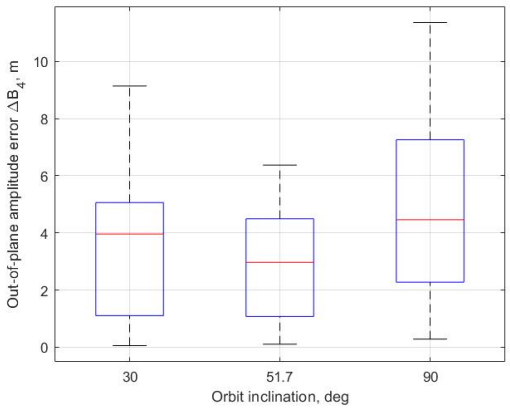

(b) Mean error in B_4 after the convergence.

Figure 5.15: In-plane and Out-of-plane motion amplitude ranges mean errors when subjected to different orbital plane inclination values.

5.4 Two-controlled satellite study case

In the second case, consider the previous controlling algorithm example but applied to a case where, instead of one active satellite, there are two satellites equipped with onboard charge changing devices, i.e., both satellites are capable to accumulate the necessary charge for the required control value. Consider a control implementation in a consensual centralized manner: both satellites are aiming to achieve a required position in the relative trajectory using the difference between the two Lorenz forces acting on both satellites. In such a case the control capacity shall increase, once there are two satellites capable of controlling the relative distance. The calculated control is implemented in the two satellites and its characterized by charges of different signs.

For this study case, the computational simulation will therefore consider a situation with two controlled satellites. The same initial conditions are randomly generated and the same parameters of the control algorithm as for the previous case are defined. The only difference is that both satellites are charging capable, and thus able to produce the Lorenz force accordingly to the required control value for the trajectory correction.

Fig. 5.16 demonstrates the relative trajectory of the two controlled satellites during a simulation with a period of 120 hours. Fig. 5.17 and 5.18 show the required and the actual values of the trajectory B parameters.

From these plots, it can be concluded that for the two active satellites control scheme, the transition between the first and the second stages of the control algorithm took about 10 hours when either B_1 and B_3 values achieve the vicinity of the required values.

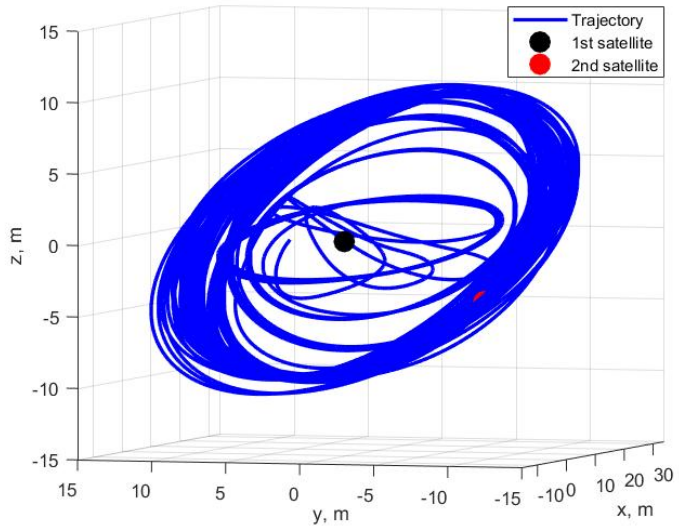

Figure 5.16: Relative trajectory under control.

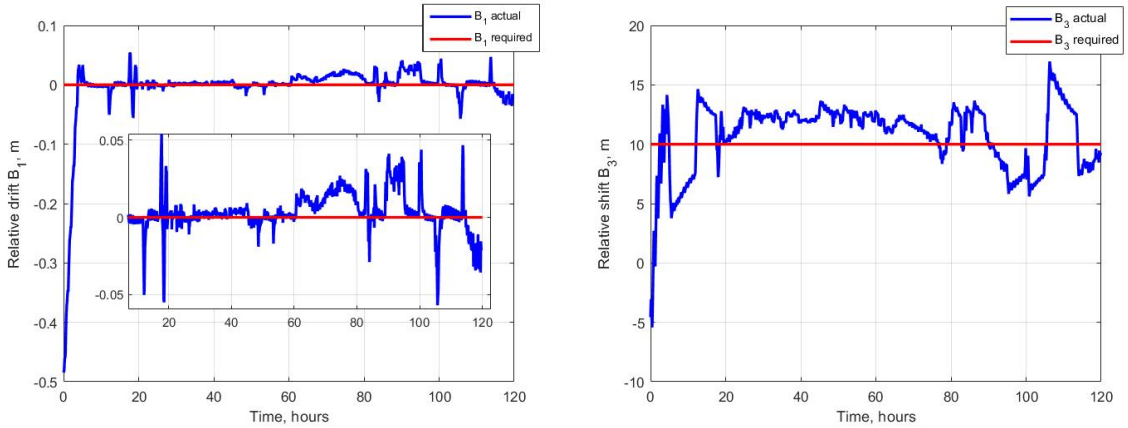

(a) Relative drift.

(b) Relative shift.

Figure 5.17: The relative drift and relative shift results

Comparing to the previous case with one active satellite, it took less than 5 hours to achieve this convergence. As for the second stage, similarly to the first stage, it took about the same 10 hours until the convergence. Relatively to the in-plane amplitude motion, it converged to the required value faster than in the case of the one charged satellite. However, on the contrary, the out-of-plane amplitude convergence decreased, achieving the required value vicinity only after 80 hours of simulation. A fact that can be explained by the increased value of the disturbances, once for this case there are two satellites continuously varying their position, a factor that affects control implementation and influences the out-of-plane control performance.

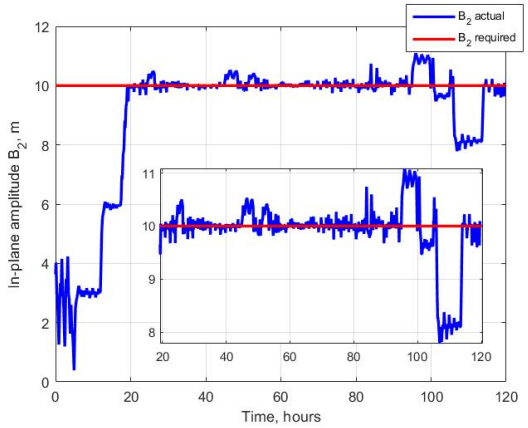

(a) In-plane motion amplitude.

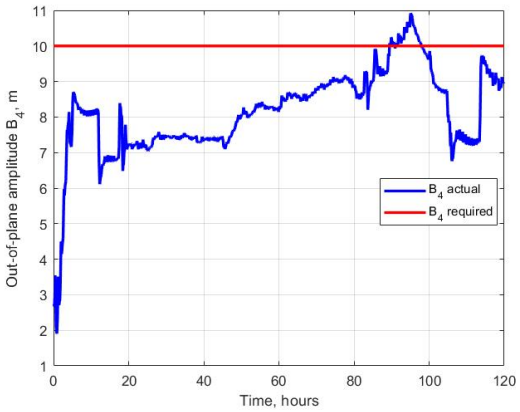

(b) Out-of-plane motion amplitude.

Figure 5.18: The in-plane and out-of-plane motion amplitude results for the formation case with two charging capable satellites for a period of 5 days after the orbital launch

Fig. 5.19 represent the charge variation of the two satellites. It can be seen that in the case of two controlled satellites the charge saturation of the onboard device is rarely witnessed, since the required control is implemented through the difference between the Lorentz forces of the two satellites, which have the same amplitude but the opposite sign.

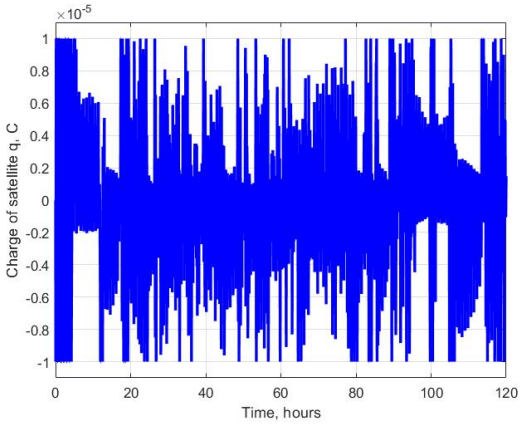

(a) Charge variation values through the control action period for the 1st satellite.

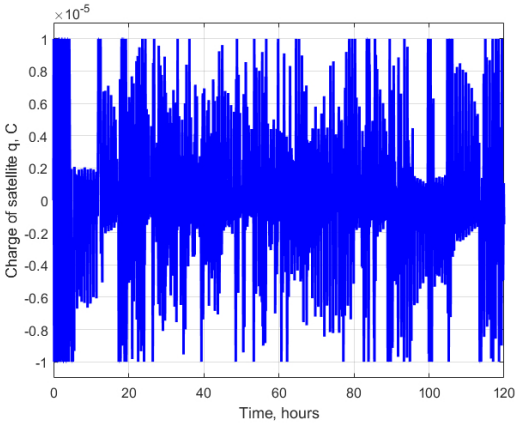

(b) Charge variation values through the control action period for the 2nd satellite.

Figure 5.19: Charging variation and the application of the variation filter

5.5 Swarm case

For the third and last formation case, the proposed control algorithm is applied for a formation flying consisting of a large number of satellites. A satellite swarm can be used as a spatially distributed measurement system in LEO. Let's consider then two distinct examples of a swarm distribution of nanosatellites, being controlled using the proposed control algorithm. The first configuration example is a formation that consists of N satellites (where N stands as a determined number of satellites) where all the elements are configured to achieve

a position with null relative drift and shift value concerning the centrally positioned virtual satellite, however, having different in-plane amplitude sizes adjusted. Such configurations are useful for the construction of spatial measurement systems in space, able to perform their missions with a higher success rate. As for the second configuration example, it is a sort of train-like formation, where all the satellites are distributed with the same relative distance in the along-track direction along the orbital path. This is a useful type of formation considering missions designed for Earth-remote sensing problems.

5.5.1 Nested Ellipses

Consider a formation flying consisting of 5 satellites, though the total number of the swarm elements could be larger without affecting algorithm performance yet turning it difficult to present the resultant relative trajectories, therefore motivating the usage of a swarm with only 5 elements for the simulations. Concerning the initial terms, the same conditions are implemented, as presented in Table 1, except for the required values to be achieved in trajectory constants. The required drift and shift is set to zero for every satellite in the formation, $B_1 = 0$ and $\Delta B_3 = 0$, as the out-of-plane amplitude value is also set constant $\Delta B_4 = 0$. To construct the spatially distributed system the required value for the in-plane amplitude differs by 10 meters from satellite to satellite. So, this results in a construction that places the five different satellites in singular independent orbits, nested as ellipses of various sizes.

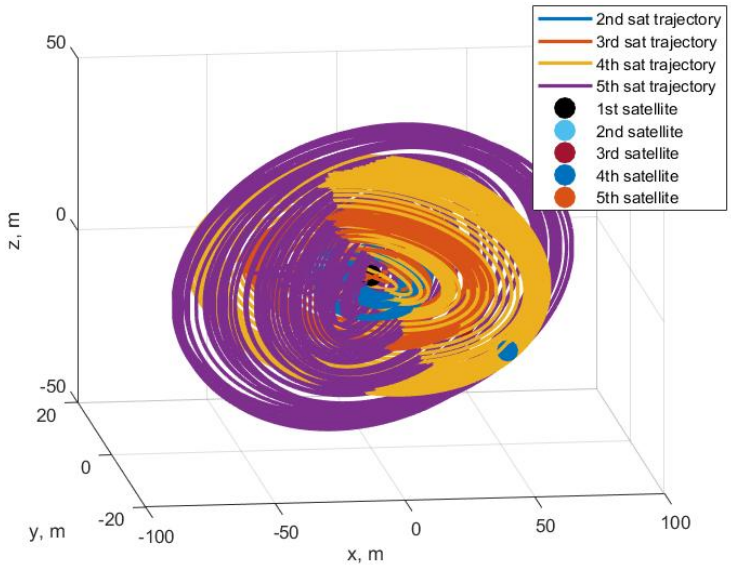

Figure 5.20: Relative trajectories for the Nested Ellipses swarming case.

Fig. 5.20 depicts an example of the relative trajectories of 5 satellites during a 120 hours period of simulation, and Fig. 5.21 presents the resulting trajectories after convergence, presenting a clear view of the final configuration achieved. As it is possible to verify, the control algorithm is able to successfully fulfill the not only required trajectory for each of the satellites but also to establish the proposed configuration with the required size of the ellipses nested inside each other.

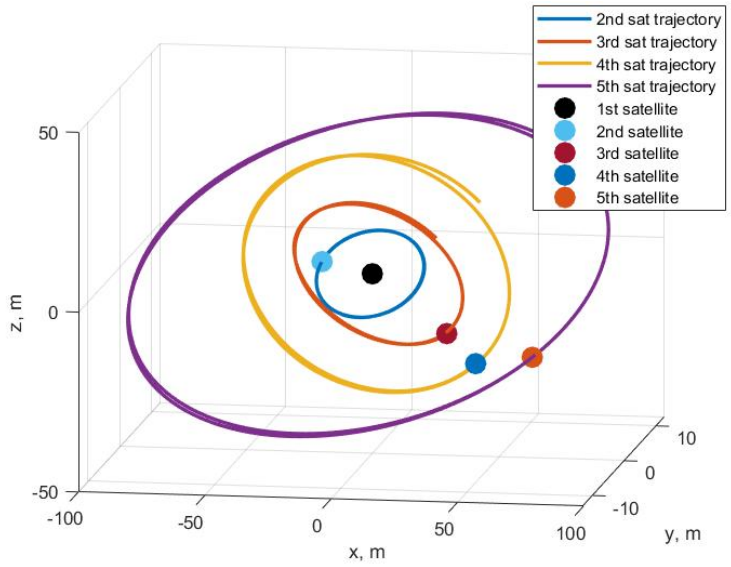

Figure 5.21: Relative trajectories for Nested Ellipses the swarming case during the last 2 hours of simulation.

Fig. 5.22 present the relative drift and shift measured for each of the formation satellites and it is possible to verify that every element achieves and maintains a relative position with both B_1 and B_3 in the vicinity of the required zero value.

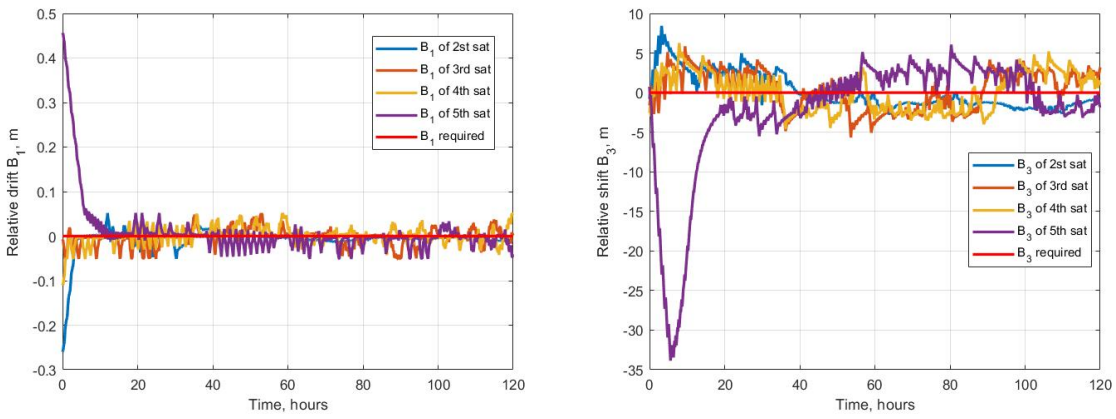

(a) Relative drift for the Nested Ellipses case. (b) Relative shift for the Nested Ellipses case.

Figure 5.22: Relative drift and shift for the Nested Ellipses swarming case.

From Fig. 5.23a it is possible to confirm the convergence of the in-plane amplitudes to the required values. It is also important to note that with larger in-plane amplitudes the longer it takes to achieve the required position in the configuration, therefore explaining the reason for the 5th satellite to take almost 100 hours to get to the required position, distanced 40 meters from the ellipse center. The errors in out-of-plane amplitudes are up to 4 m after convergence as one can see in Fig. 5.23b.

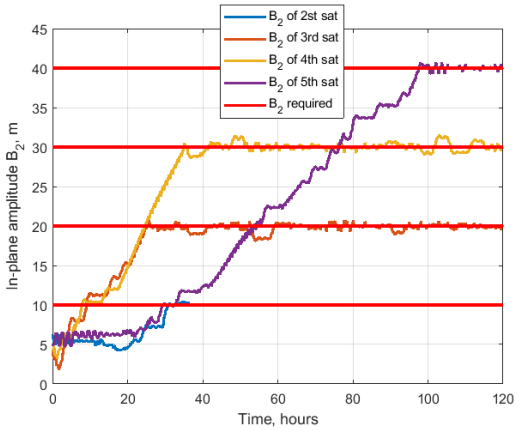

(a) In-plane amplitude motion for the Nested Ellipses case.

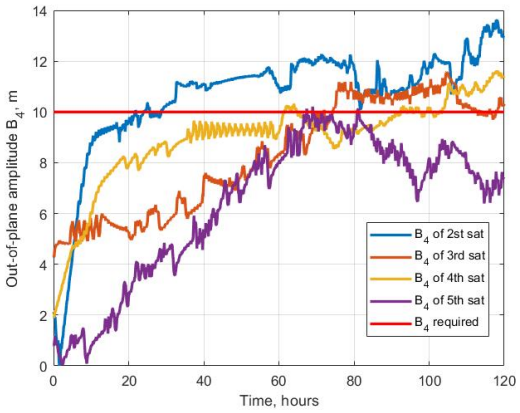

(b) Out-of-plane amplitude motion for the Nested Ellipses case.

Figure 5.23: In-plane and Out-of-plane motion amplitudes for the Nested Ellipses swarming case.

In the presented example the implemented control strategy used was the centralized approach, where all the satellites are following the motion of a chief satellite centered in the planned orbital path, and which, in this case, is the first satellite to be deployed and that is represented as the black dot. Since the phase of the satellites is not controllable, the satellites present a random position distribution along the ellipses and the planes of the ellipses do not coincide.

5.5.2 Train Formation

The train formation is used when uniformly distributed measurements along the same orbit are required for the mission. To achieve such a configuration using the developed control algorithm, the required shift values, B_3, should be of similar magnitude for all the elements, while the other parameters shall converge to zero. Considering a formation that is consisted of the same 5 satellites, as the previous example and taking the same simulation beginning parameters. For this case, the control strategy implemented can be based on the decentralized approach. Each satellite tries to achieve the required B_3 value, i.e., the required orbit shift relative to the closest neighbors, following the orbital track of the satellite with the smallest positive shift value ($B_3 = 0$). Fig. 5.24 shows the example of the relative trajectories of 5 satellites during a simulation of 120 hours, and Fig. 5.25 presents the resulting trajectories after convergence.

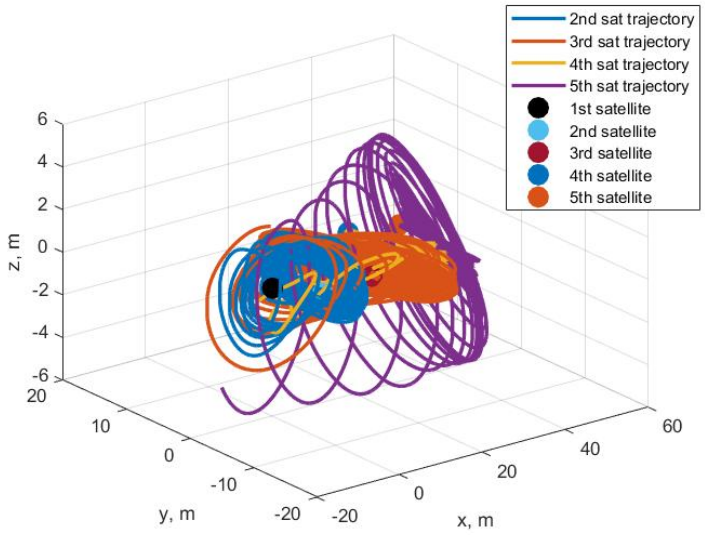

Figure 5.24: Relative trajectories for the Train Formation swarming case.

As it is possible to verify in the graphics, after a certain time period all the elements in the formation present a lined up configuration, in the along-track direction and with a separation of 10 meters between each satellite. Except for the out-of-plane amplitudes, that reach a total distancing of about 5 meters by the end of the simulation, all the other B parameters converge to the required zero value.

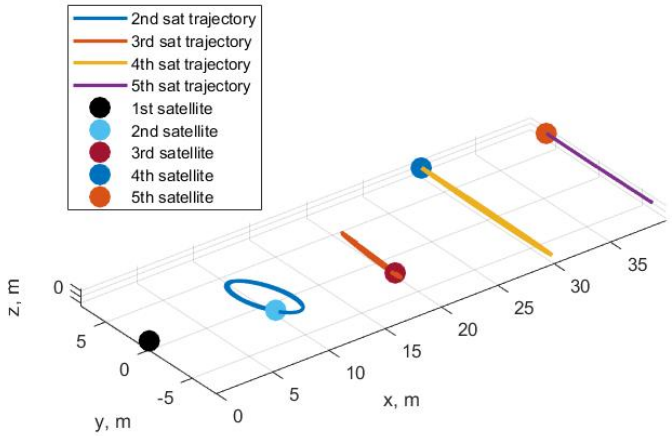

Figure 5.25: Relative trajectories for the Train Formation swarming case during the last 2 hours of simulation.

Fig. 5.26 and 5.27 present the values of the convergence of the parameters. The relative drift is close to zero value, while the relative shifts are all at the required values presenting a distance of 10 meters of difference.

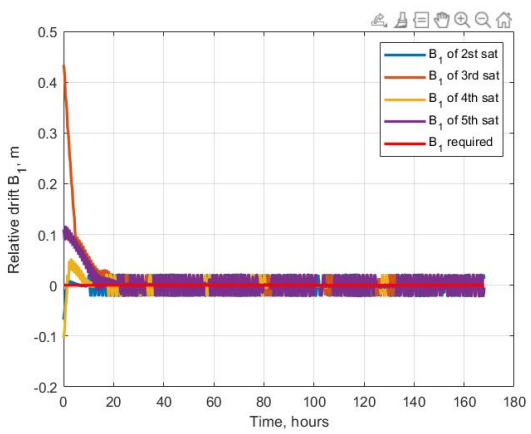

(a) Relative drift of the Train Formation for the swarming case.

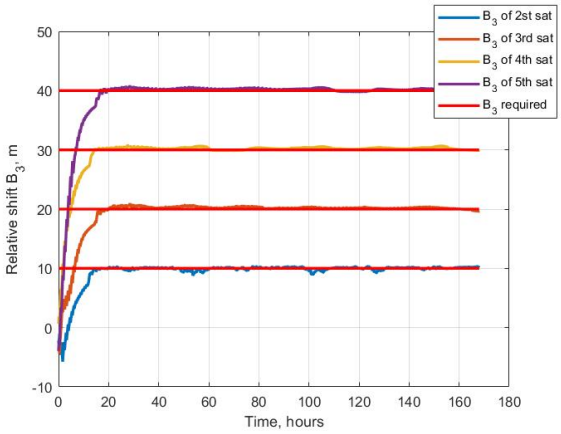

(b) Relative shift of the Train Formation for the swarming case.

Figure 5.26: Relative Drift and shift for the Train Formation case.

For a perfect train configuration, all the amplitudes should converge to a zero, a fact that is accomplished when considering the in-plane amplitudes, once these are almost all converged to zero after 160 hours of simulation, nonetheless when considering the out-of-plane motion this convergence is even slower. After 160 hours of simulation, there is an error of several meters.

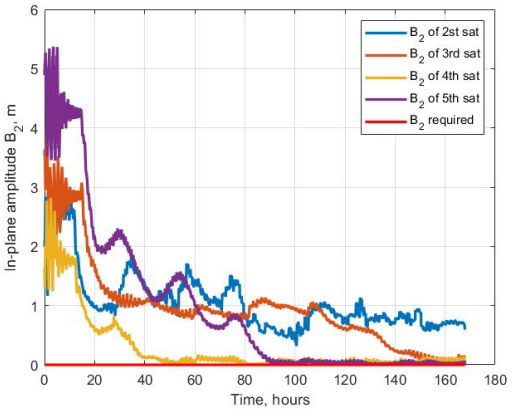

(a) In-plane amplitude motion for the Train Formation swarming case.

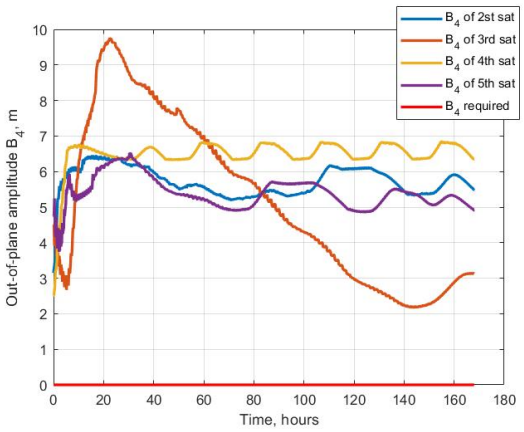

(b) Out-of-plane amplitude motion for the Train Formation swarming case.

Figure 5.27: In-plane and Out-of-plane motion for the Train Formation case.

Fig. 5.28 demonstrates the charges of the satellites. All the values are kept at the maximum value and after convergence, these values rarely achieve the respective constraints.

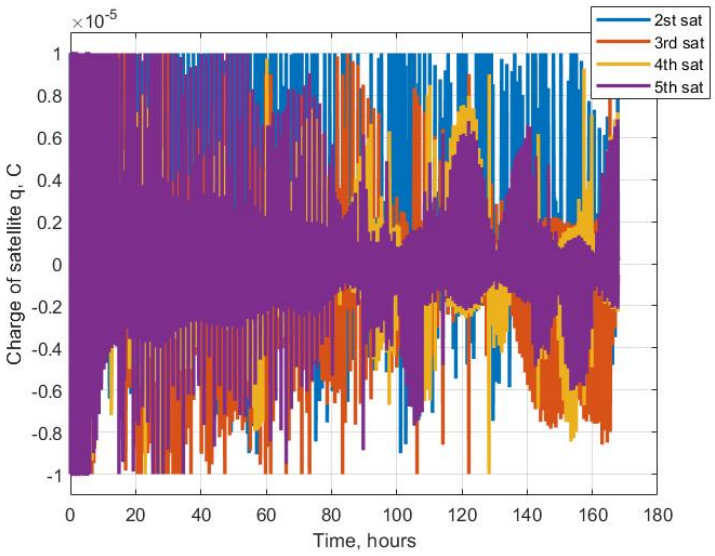

Figure 5.28: Charge changing behavior for the Train Formation swarming case.

Thus, the examples proposed for the algorithm application on the construction and maintenance of the two swarm configurations, consisting of a cluster of multiple satellites, validates the usage of the algorithm for this kind of formations and even demonstrates its excellent performance. All the trajectories converged to the required ones with final error of several meters.

Chapter 6

Conclusion

A control algorithm based on the Lorentz force application is developed for the problems of construction and maintenance of the relative motion of a small satellites formation flying. For Lorentz force application, an onboard charging device that is capable to provide the required charge is considered. There are only 4 of the 6 total state vector elements that are controllable, since the Lorentz force vector direction is defined by the local Geomagnetic field and by the orbital velocity. Concerning the relative trajectory parameters, the proposed Lyapunov-based control goal is to achieve a null relative drift value, while converging to the required relative shift, in-plane, and out-of-plane trajectory amplitudes. The in-plane and out-of-plane motion phases are considered to be uncontrollable. However, the required relative configurations, when considering the size and shape of the proposed formations, are achieved by the developed control. The numerical study showed that the best algorithm performance could be achieved at orbital inclinations that are near the polar plane. The initial conditions and the maximum possible charge affect the time required for convergence as well as the trajectory errors after the convergence instant. Out-of-plane amplitude errors are the most significant among the errors obtained for the other parameters. The results of the application of the proposed algorithm are demonstrated in three formation cases: the first case consists of one controlled satellite in a two-satellite formation flying, the second one with two controlled satellites, and lastly two different configurations for a multiple satellite formation flying, distinguished as nested ellipses and train configurations. The control algorithm revealed to be successful among all the cases studied, being able to achieve the required trajectories, although presenting final errors of several meters for some relative orbital parameters. The proposed Lorentz force control offers a renewed perspective on relative positioning in flying formations by applying an onboard charging capable device in the small satellites, therefore not requiring any fuel consumption. The relative drift is close to zero value, while the relative shifts are all at the required values presenting a distance of 10 meters of difference. Further investigation of the Lorentz force formation flying control should consider the relative attitude motion to study the influence of torque disturbances caused by the onboard charge. Another field perspective of the research is to utilize both Lorentz force and differential drag for formation flying control in LEO.

Bibliography

[1] C. Cappelletti, S. Battistini, and B. Malphrus, *Cubesat Handbook: From Mission Design to Operations*, 1st ed. Academic Press, 2020.

[2] G. Amaro, D. Ivanov, and A. Guerman, "Formation flying control of the relative trajectory shape and size using lorenz forces," *Proceeding of IAC-21, Paper IAC-21-C1.1.12*, p. 15, 2021.

[3] Jorge Emanuel Teló Bordalo Monteiro, "Mission analysis and design of mecse nanosatellite," Master Thesis, Universidade da Beira Interior, 10/2017.

[4] SpaceWorks, "2020 nano/microsatellite market forecast, 10th edition." [Online]. Available: https://www.spaceworks.aero/nano-microsatellite-forecast-10th-edition-2020/ (Accessed: 16/08/2021).

[5] A. Toorian, K. Diaz, and S. Lee, "The cubesat approach to space access," in *2008 IEEE Aerospace Conference*, 2008, pp. 1–14.

[6] X. Roser, F. Arbusti, X. Leyre, and M. Sghedoni, *Formation flying enabling technologies for a big leap in science missions and perspectives for space projects*. AIAA, 2016. [Online]. Available: https://arc.aiaa.org/doi/abs/10.2514/6.IAC-06-D1.4.05

[7] J. S. Peter Fortescue, Graham Swinerd, *Spacecraft Systems Engineering (Aerospace Series)*, 4th ed. Wiley, 2011.

[8] J. R. W. Wiley J. Larson, *Space Mission Analysis and Design*, 3rd ed., ser. Space Technology Library. Microcosm, 2005.

[9] A. Lahrichi, "Different cubesat frame sizes." [Online]. Available: https://www.researchgate.net/figure/Different-CubeSat-Frame-Sizes_fig1_330225008 (Accessed: 16/08/2021).

[10] Jaime L. Ramirez Riberos, "New decentralized algorithms for spacecraft formation control based on a cyclic approach," Thesis (Ph. D.), Massachusetts Institute of Technology. Department of Aeronautics and Astronautics., 2010.

[11] K. T. Alfriend, S. R. Vadali, J. P. H. Pini Gurfil, and L. S. Berger, *Spacecraft Formation Flying, Dynamics, Control and navigation*, 1st ed., ser. Elsevier Astrodynamics Series. Elsevier, 2010.

[12] E. M. C. Kong, D. W. Kwon, S. A. Schweighart, L. M. Elias, R. J. Sedwick, and D. W. Miller, "Electromagnetic formation flight for multisatellite arrays," *Journal of Spacecraft and Rockets*, vol. 41, no. 4, pp. 659–666, 2004. [Online]. Available: https://doi.org/10.2514/1.2172

[13] C. Saaj, V. Lappas, D. Richie, M. Peck, B. J. Streetman, and H. Schaub, "Electrostatic forces for satellite swarm navigation and reconfiguration final report," 2006.

[14] D. Scharf, F. Hadaegh, and S. Ploen, "A survey of spacecraft formation flying guidance and control (part 1): guidance," in *Proceedings of the 2003 American Control Conference, 2003.*, vol. 2, 2003, pp. 1733–1739.

[15] F. Hadaegh, G. Singh, B. Açıkmeşe, D. Scharf, and M. Mandić, "Guidance and control of formation flying spacecraft," *In The Path to Autonomous Robots*, pp. 1–19, 01 2009.

[16] D. Scharf, F. Hadaegh, and S. Ploen, "A survey of spacecraft formation flying guidance and control. part ii: control," in *Proceedings of the 2004 American Control Conference*, vol. 4, 2004, pp. 2976–2985 vol.4.

[17] R. Burns, C. McLaughlin, J. Leitner, and M. Martin, "Techsat 21: formation design, control, and simulation," in *2000 IEEE Aerospace Conference. Proceedings (Cat. No.00TH8484)*, vol. 7, 2000, pp. 19–25.

[18] P. K. C. Wang, F. Y. Hadaegh, and K. Lau, "Synchronized formation rotation and attitude control of multiple free-flying spacecraft," *Journal of Guidance, Control, and Dynamics*, vol. 22, no. 1, pp. 28–35, 1999. [Online]. Available: https://doi.org/10.2514/2.4367

[19] H. Pan and V. Kapila, "Adaptive nonlinear control for spacecraft formation flying with coupled translational and attitude dynamics," in *Proceedings of the 40th IEEE Conference on Decision and Control (Cat. No.01CH37228)*, vol. 3, 2001, pp. 2057–2062 vol.3.

[20] E. Davison, "The decentralized stabilization and control of a class of unknown nonlinear time-varying systems," *Automatica*, vol. 10, no. 3, pp. 309–316, 1974. [Online]. Available: https://www.sciencedirect.com/science/article/pii/0005109874900417

[21] G. Krieger, A. Moreira, H. Fiedler, I. Hajnsek, M. Werner, M. Younis, and M. Zink, "Tandem-x: A satellite formation for high-resolution sar interferometry," *IEEE Transactions on Geoscience and Remote Sensing*, vol. 45, no. 11, pp. 3317–3341, 2007.

[22] E. Gill, S. D'Amico, and O. Montenbruck, "Autonomous formation flying for the prisma mission," *Journal of Spacecraft and Rockets*, vol. 44, no. 3, pp. 671–681, 2007.

[Online]. Available: https://doi.org/10.2514/1.23015

[23] S. Vivès, P. Lamy, P. Levacher, M. Venet, and J. L. Boit, "In-flight validation of the formation flying technologies using the ASPIICS/PROBA-3 giant coronagraph," in *Space Telescopes and Instrumentation 2008: Optical, Infrared, and Millimeter*, ser. Society of Photo-Optical Instrumentation Engineers (SPIE) Conference Series, J. Oschmann, Jacobus M., M. W. M. de Graauw, and H. A. MacEwen, Eds., vol. 7010, Jul. 2008, p. 70103R.

[24] J. Llorente, A. Agenjo, C. Carrascosa, C. de Negueruela, A. Mestreau-Garreau, A. Cropp, and A. Santovincenzo, "Proba-3: Precise formation flying demonstration mission," *Acta Astronautica*, vol. 82, no. 1, pp. 38–46, 2013, 6th International Workshop on Satellite Constellation and Formation Flying. [Online]. Available: https://www.sciencedirect.com/science/article/pii/S0094576512002202

[25] D. Ivanov, U. Monakhova, A. Guerman, M. Ovchinnikov, and D. Roldugin, "Decentralized differential drag based control of nanosatellites swarm spatial distribution using magnetorquers," *Advances in Space Research*, vol. 67, no. 11, pp. 3489–3503, 2021, satellite Constellations and Formation Flying. [Online]. Available: https://www.sciencedirect.com/science/article/pii/S0273117720303471

[26] D. Mishne, "Formation control of satellites subject to drag variations and j2 perturbations," *Journal of Guidance, Control, and Dynamics*, vol. 27, no. 4, pp. 685–692, 2004. [Online]. Available: https://doi.org/10.2514/1.11156

[27] Y. Mashtakov, M. Ovchinnikov, T. Petrova, and S. Tkachev, "Two-satellite formation flying control by cell-structured solar sail," *Acta Astronautica*, vol. 170, pp. 592–600, 2020. [Online]. Available: https://www.sciencedirect.com/science/article/pii/S0094576520300862

[28] D. Ivanov, M. Kushniruk, and M. Ovchinnikov, "Study of satellite formation flying control using differential lift and drag," *Acta Astronautica*, vol. 152, pp. 88–100, 2018. [Online]. Available: https://www.sciencedirect.com/science/article/pii/S009457651830540X

[29] D. Folta, L. Newman, and T. Gardner, *Foundations of formation flying for Mission to Planet Earth and New Millennium*. AIAA, 1996. [Online]. Available: https://arc.aiaa.org/doi/abs/10.2514/6.1996-3645

[30] M. Peck, *Prospects and Challenges for Lorentz-Augmented Orbits*. AIAA Guidance, Navigation, and Control Conference, 2005. [Online]. Available: https://arc.aiaa.org/doi/abs/10.2514/6.2005-5995

[31] L. Schaffer and J. Burns, "Charged dust in planetary magnetospheres: Hamiltonian dynamics and numerical simulations for highly charged grains," *Journal of Geophysical Research*, vol. 99, pp. 17 211–17 223, 1994.

[32] Wikipedia, "Magnetic deflection helical path." [Online]. Available: https://commons.wikimedia.org/wiki/File:Magnetic_deflection_helical_path.svg (Accessed: 16/08/2021).

[33] D. Kwon, "Propellantless formation flight applications using electromagnetic satellite formations," *Acta Astronautica*, vol. 67, pp. 1189–1201, 11 2010.

[34] X. Huang, Y. Yan, and Y. Zhou, "Optimal spacecraft formation establishment and reconfiguration propelled by the geomagnetic Lorentz force," *Advances in Space Research*, vol. 54, no. 11, pp. 2318–2335, Dec. 2014.

[35] Y. Abdel-Aziz and M. Shoaib, "Attitude dynamics and control of spacecraft using geomagnetic lorentz force," *Research in Astronomy and Astrophysics*, 01 2015.

[36] C. Peng and Y. Gao, "Lorentz-force-perturbed orbits with application to j2-invariant formation," *Acta Astronautica*, vol. 77, p. 12–28, 08 2012.

[37] H. Yamakawa, M. Bando, K. Yano, and S. Tsujii, "Spacecraft relative dynamics under the influence of geomagnetic lorentz force," in *AIAA/AAS Astrodynamics Specialist Conference 2010*, ser. AIAA/AAS Astrodynamics Specialist Conference 2010, 2010, funding Information: This research is supported by the Grant-in-Aid for Challenging Exploratory Research (No. the Japan Society for Promotion of Science.; AIAA/AAS Astrodynamics Specialist Conference 2010 ; Conference date: 02-08-2010 Through 05-08-2010.

[38] S. Tsujii, M. Bando, and H. Yamakawa, "Spacecraft formation flying dynamics and control using the geomagnetic lorentz force," *Journal of Guidance, Control, and Dynamics*, vol. 36, pp. 136–148, 01 2013.

[39] J. J. H. Schaub, *Analytical Mechanics of Space Systems*, 2nd ed., ser. AIAA Education Series. AIAA, 2009.

[40] H. D. Curtis, *Orbital Mechanics For Engineering Students*, 4th ed., ser. Elsevier Aerospace Engineering Series. Elsevier/Butterworth-Heinemann, 2020.

[41] J. W. e. David A. Vallado, *Fundamentals of Astrodynamics and Applications*, 4th ed., ser. Space Technology Library. Microcosm Press, 2013.

[42] J. E. W. Roger R. Bate, Donald D. Mueller, *Fundamentals of astrodynamics*, 1st ed.

Dover Publications, 1971.

[43] D. E. G. a. Dr. Oliver Montenbruck, *Satellite Orbits: Models, Methods and Applications*, 1st ed. Springer-Verlag Berlin Heidelberg, 2000.

[44] E. S. A. (ESA), "Earth's geoid as seen by goce." [Online]. Available: https://www.esa.int/ESA_Multimedia/Images/2008/05/Earth_s_geoid_as_seen_by_GOCE (Accessed: 16/08/2021).

[45] B. G. Survey, "International geomagnetic reference field (igrf)." [Online]. Available: https://geomag.bgs.ac.uk/research/modelling/IGRF.html (Accessed: 16/08/2021).

[46] C. Finlay, *Models of the Main Geomagnetic Field Based on Multi-satellite Magnetic Data and Gradients—Techniques and Latest Results from the Swarm Mission*. Springer, 10 2019, pp. 255–284.

[47] X. Huang, Y. Yan, and Y. Zhou, "Optimal lorentz-augmented spacecraft formation flying in elliptic orbits," *Acta Astronautica*, vol. 111, 07 2015.

[48] D. R. M. (auth.), *Introduction to the Theory of Stability*, 1st ed., ser. Texts in Applied Mathematics 24. Springer-Verlag New York, 1996.

[49] E. Barbashin, "The construction of lyapunov functions for non-linear systems," *IFAC Proceedings Volumes*, vol. 1, no. 1, pp. 953–957, 1960.

[50] A. Y. Aleksandrov, "On the construction of lyapunov functions for nonlinear systems," *Differential Equations*, vol. 41, no. 3, pp. 303–309, 2005.

Appendix A

Anexos

A.1 Hill-Clohessy-Wiltshire Equations

A.1.1 Linearization of the HCW equations

There are different methods to derive the HCW equations available in literature. The method applied here is described as in more detail in [[40]]. To begin, consider two satellites in a Leader/Follower configuration orbiting the Earth. Let $\mathbf{R_1}$ and $\mathbf{R_2}$ be the position vectors of the Leader and the Follower, respectively, in the ECI reference frame. And let $\mathbf{R_{12}}$ be the relative position vector of the follower relative to the leader, expressed in the ECI reference frame. Note that $\mathbf{R_{12}}$ is of much smaller magnitude than $\mathbf{R_1}$ or $\mathbf{R_2}$, so that

$$\frac{||\mathbf{R_{12}}||}{||\mathbf{R_1}||} \ll 1 \tag{A.1}$$

The relative position vector of the follower can be defined as,

$$\mathbf{R_2} = \mathbf{R_1} + \mathbf{R_{12}} \tag{A.2}$$

From Eq.3.14 the equation of motion for the two bodies is determined,

$$\begin{aligned} \ddot{\mathbf{R}}_{\mathbf{2}} &= -\mu \frac{\mathbf{R_2}}{||\mathbf{R_2}||^3} \\ \ddot{\mathbf{R}}_{\mathbf{12}} &= -\ddot{\mathbf{R}}_{\mathbf{1}} - \mu \frac{\mathbf{R_1} + \mathbf{R_{12}}}{||\mathbf{R_1} + \mathbf{R_{12}}||^3} \end{aligned} \tag{A.3}$$

It is known from Eq.A.1, that $||\mathbf{R_{12}}||$ is a comparatively small value, therefore all powers of $\frac{||\mathbf{R_{12}}||}{||\mathbf{R_1}||}$ greater the the unity can be neglected in order to simplify into Eq.3.14. First note that,

$$
\begin{aligned}
||\mathbf{R_2}||^2 &= ||\mathbf{R_1} + \mathbf{R_2}||^2 \\
&= \mathbf{R_1} \cdot \mathbf{R_2} \\
&= (\mathbf{R_1} + \mathbf{R_{12}}) \cdot (\mathbf{R_1} + \mathbf{R_{12}}) \\
&= \mathbf{R_1} \cdot \mathbf{R_1} + 2\mathbf{R_1} \cdot \mathbf{R_{12}} + \mathbf{R_{12}} \cdot \mathbf{R_{12}}
\end{aligned}
\tag{A.4}
$$

The term $\mathbf{R_1} \cdot \mathbf{R_1} = ||\mathbf{R_{12}}||^2$ can be factored out yielding,

$$
||\mathbf{R_1} + \mathbf{R_{12}}||^2 = ||\mathbf{R_1}||^2 \left[1 + \frac{2\mathbf{R_1} \cdot \mathbf{R_{12}}}{||\mathbf{R_1}||^2} + (\frac{||\mathbf{R_{12}}||}{||\mathbf{R_1}||})^2\right] \tag{A.5}
$$

The term $\left(\frac{||\mathbf{R_{12}}||}{||\mathbf{R_1}||}\right)^2$ is neglected by virtue of Eq.A.1,

$$
||\mathbf{R_1} + \mathbf{R_{12}}||^2 = ||\mathbf{R_1}||^2 \left[1 + \frac{2\mathbf{R_1} \cdot \mathbf{R_{12}}}{||\mathbf{R_1}||^2}\right] \tag{A.6}
$$

Since,

$$
||\mathbf{R_2}||^{-3} = \left(||\mathbf{R_2}||^2\right)^{-\frac{3}{2}} \tag{A.7}
$$

$$
||\mathbf{R_1} + \mathbf{R_{12}}||^{-3} = ||\mathbf{R_1}||^{-3} \left[1 + \frac{2\mathbf{R_1} \cdot \mathbf{R_{12}}}{||\mathbf{R_1}||^2}\right]^{-\frac{3}{2}} \tag{A.8}
$$

Applying the binomial expansion theorem from [H.D.Curtis, p.378]:

$$
(a+b)^n = a^n + n \cdot a^{n-1} \cdot b + \frac{n(n-1)}{2!} a^{n-2} \cdot b^2 + \frac{n(n-1)(n-2)}{3!} a^{n-3} \cdot b^3 + \ldots \tag{A.9}
$$

$$\left(1+\frac{2\mathbf{R_1}\cdot\mathbf{R_{12}}}{||\mathbf{R_1}||^2}\right)^{-\frac{3}{2}}=1+\left(-\frac{3}{2}\right)\left(\frac{2\mathbf{R_1}\cdot\mathbf{R_{12}}}{||\mathbf{R_1}||^2}\right) \tag{A.10}$$

Then Eq.A.7 becomes,

$$\begin{gathered}||\mathbf{R_1}+\mathbf{R_{12}}||^{-3}=||\mathbf{R_1}||^{-3}\left(1-\frac{3\mathbf{R_1}\cdot\mathbf{R_{12}}}{||\mathbf{R_1}||^2}\right)\\ \frac{1}{||\mathbf{R_1}+\mathbf{R_{12}}||^3}=\frac{1}{||\mathbf{R_1}||^3}-\frac{1}{||\mathbf{R_1}||^5}\mathbf{R_1}\cdot\mathbf{R_{12}}\end{gathered} \tag{A.11}$$

Substituting Eq.A.11 into Eq.A.3 yields,

$$\ddot{\mathbf{R}}_{12}=-\ddot{\mathbf{R}}_1-\mu\left(\frac{1}{||\mathbf{R_1}||^3}-\frac{1}{||\mathbf{R_1}||^5}\mathbf{R_1}\cdot\mathbf{R_1}\right)(\mathbf{R_1}+\mathbf{R_{12}})$$

$$\ddot{\mathbf{R}}_{12}=-\ddot{\mathbf{R}}_1-\mu\left[\frac{\mathbf{R_1}+\mathbf{R_{12}}}{||\mathbf{R_1}||^3}-\frac{1}{||\mathbf{R_1}||^5}(\mathbf{R_1}\cdot\mathbf{R_{12}})(\mathbf{R_1}+\mathbf{R_{12}})\right]$$

$$\ddot{\mathbf{R}}_{12}=-\ddot{\mathbf{R}}_1-\mu\left[\frac{\mathbf{R_1}}{||\mathbf{R_1}||^3}+\frac{\mathbf{R_{12}}}{||\mathbf{R_1}||^3}-\frac{1}{||\mathbf{R_1}||^5}(\mathbf{R_1}\cdot\mathbf{R_{12}})\mathbf{R_1}+H.O.T.\right]$$

$$\ddot{\mathbf{R}}_{12}=-\ddot{\mathbf{R}}_1-\mu\frac{\mathbf{R_1}}{||\mathbf{R_1}||^3}-\frac{\mu}{||\mathbf{R_1}||^3}\left[\mathbf{R_{12}}-\frac{3}{||\mathbf{R_{12}}||^2}(\mathbf{R_1}\cdot\mathbf{R_{12}})\mathbf{R_1}\right] \tag{A.12}$$

The equation of motion Eq.3.14 of the leader is:

$$\ddot{\mathbf{R}}_1=-\frac{\mu}{r^3}\mathbf{R_1} \tag{A.13}$$

Substituting it into Eq.A.12 yields the simplified equation of the two-body system,

$$\ddot{\mathbf{R}}_{12}=-\frac{\mu}{||\mathbf{R_1}||^3}\left[\mathbf{R_{12}}-\frac{3}{||\mathbf{R_1}||^2}(\mathbf{R_1}\cdot\mathbf{R_{12}})\mathbf{R_1}\right] \tag{A.14}$$

This expression is a linear approximation of the motion of the follower relative to the leader, obtained by dropping the negligible terms,which is only valid if the Eq.A.1 is true. In the rotating Hill frame (established in section 3.3), the z-axis lies along the radial $\mathbf{R_1}$, so that,

$$\mathbf{R_1} = R_1\mathbf{k} \tag{A.15}$$

where $R_1 = ||\mathbf{R_1}||$. The components of the relative position vector in the co-moving frame can be defined as,

$$\ddot{\mathbf{R}}_{\mathbf{1}} = x_{12}\mathbf{i} + y_{12}\mathbf{j} + z_{12}\mathbf{k} \tag{A.16}$$

Substituting Eq.A.15 an Eq.A.16 into Eq.A.14 yields,

$$\begin{aligned}\ddot{\mathbf{R}}_{\mathbf{12}} &= -\frac{\mu}{R_1^3}\left[x_{12}\mathbf{i} + y_{12}\mathbf{j} + z_{12}\mathbf{k} - \frac{3}{R_1^2}\left(R_1\mathbf{k}\cdot(x_{12}\mathbf{i} + y_{12}\mathbf{j} + z_{12}\mathbf{k})\right)R_1\mathbf{k}\right] \\ &= -\frac{\mu}{R_1^3}(x_{12}\mathbf{i} + y_{12}\mathbf{j} + z_{12}\mathbf{k})\end{aligned} \tag{A.17}$$

The equation obtained corresponds to the acceleration of the follower relative to the leader, measured in the ECI frame. From Eq.(3.36) it is determined the angular momentum is normal to the reference orbit plane, and so is the y-plane of the Hill reference frame. Since (?), the angular velocity and angular acceleration of the leader from Eq.(3.25) can be written as,

$$\begin{aligned}\omega &= \frac{\mathbf{R}_1 \times \mathbf{V}_1}{R_1^2}\mathbf{j} \\ &= \frac{h}{R_1^2}\mathbf{j}\end{aligned} \tag{A.18}$$

$$\dot{\omega} = -\frac{2(\mathbf{R}_1\cdot\mathbf{V}_1)h}{R_1^4}\mathbf{j} \tag{A.19}$$

where $\mathbf{V}_1$ is the first derivative of $\mathbf{R}_1$. The equation from [40] is applied to calculate the relative acceleration of the two bodies, measured in the Hill frame:

$$\ddot{\mathbf{r}}_{12} = \ddot{\mathbf{R}}_{12} - \dot{\omega} \times \mathbf{R}_{12} - \omega \times (\omega \times \mathbf{R}_{12}) - 2\omega \times \mathbf{v}_{12} \tag{A.20}$$

where,

$$\mathbf{r}_{12} = x_{12}\mathbf{i} + y_{12}\mathbf{j} + z_{12}\mathbf{k} \tag{A.21}$$

$$\mathbf{v}_{12} = \dot{x}_{12}\mathbf{i} + \dot{y}_{12}\mathbf{j} + \dot{z}_{12}\mathbf{k} \tag{A.22}$$

are the relative state vectors in the Hill reference frame. Substituting the Eqs.(A.16), (A.18) and (A.19) into Eq.(A.20) yields

$$\begin{aligned} \dot{\omega} \times \mathbf{R}_{12} &= \left[-\frac{2(\mathbf{R}_1 \cdot \mathbf{V}_1)h}{R_1^4}\mathbf{j} \right] \times (x_{12}\mathbf{i} + y_{12}\mathbf{j} + z_{12}\mathbf{k}) \\ &= \frac{2(\mathbf{R}_1 \cdot \mathbf{V}_1)h}{R_1^4}(z_{12}\mathbf{i} + x_{12}\mathbf{k}) \end{aligned} \tag{A.23}$$

$$\begin{aligned} \omega \times (\omega \times \mathbf{R}_{12}) &= \frac{h}{R_1^2}\mathbf{j} \times \left[\frac{h}{R_1^2}\mathbf{j} \times (x_{12}\mathbf{i} + y_{12}\mathbf{j} + z_{12}\mathbf{k}) \right] \\ &= -\frac{h^2}{R_1^4}(x_{12}\mathbf{i} + z_{12}\mathbf{k}) \end{aligned} \tag{A.24}$$

$$\begin{aligned} 2\omega \times \mathbf{v}_{12} &= 2\frac{h}{R_1^2}\mathbf{j} \times (x_{12}\mathbf{i} + y_{12}\mathbf{j} + z_{12}\mathbf{k}) \\ &= 2\frac{h}{R_1^2}(\dot{z}_{12}\mathbf{i} - \dot{x}_{12}\mathbf{k}) \end{aligned} \tag{A.25}$$

Considering Eq.(A.14), Eq.(A.17) becomes

$$\begin{aligned} \ddot{\mathbf{r}}_{12} = &-\frac{\mu}{R_1^3}(x_{12}\mathbf{i} + y_{12}\mathbf{j} - 2z_{12}\mathbf{k}) - \frac{2(\mathbf{R}_1 \cdot \mathbf{V}_1)h}{R_1^4}(-z_{12}\mathbf{i} + x_{12}\mathbf{k}) \\ &- \left[-\frac{h^2}{R_1^4}(x_{12}\mathbf{i} + z_{12}\mathbf{k}) \right] - 2\frac{h}{R_1^2}(\dot{z}_{12}\mathbf{i} - \dot{x}_{12}\mathbf{k}) \end{aligned} \tag{A.26}$$

The relative acceleration in the Hill frame is defined as

$$\ddot{\mathbf{r}}_{12} = \ddot{x}_{12}\mathbf{i} + \ddot{y}_{12}\mathbf{j} + \ddot{z}_{12}\mathbf{k} \tag{A.27}$$

and can be applied to Eq.(A.26)

$$\begin{aligned}\ddot{x}_{12}\mathbf{i} + \ddot{y}_{12}\mathbf{j} + \ddot{z}_{12}\mathbf{k} = &\left[\left(\frac{h^2}{R_1^4} - \frac{\mu}{R_1^3}\right)x_{12} + \frac{2(\mathbf{R_1}\cdot\mathbf{V_1})h}{R_1^4}z_{12} - 2\frac{h}{R_1^2}\dot{z}_{12}\right]\mathbf{i} \\ &- \left[\frac{\mu}{R_1^3}y_{12}\right]\mathbf{j} + \left[\left(\frac{h^2}{R_1^4} - \frac{\mu}{R_1^3}\right)z_{12} - \frac{2(\mathbf{R_1}\cdot\mathbf{V_1})h}{R_1^4}x_{12} + 2\frac{h}{R_1^2}\dot{x}_{12}\right]\mathbf{k}\end{aligned} \tag{A.28}$$

Eq.(A.19) can be re-arranged according to the three unit components of the relative acceleration vector,

$$\begin{cases}\ddot{x}_{12} = \left(\frac{h^2}{R_1^4} - \frac{\mu}{R_1^3}\right)x_{12} + \frac{2(\mathbf{R_1}\cdot\mathbf{V_1})h}{R_1^4}z_{12} - 2\frac{h}{R_1^2}\dot{z}_{12} \\ \ddot{y}_{12} = -\frac{\mu}{R_1^3}y_{12} \\ \ddot{z}_{12} = \left(\frac{2\mu}{R_1^3} + \frac{h^2}{R_1^4}\right)z_{12} - \frac{2(\mathbf{R_1}\cdot\mathbf{V_1})h}{R_1^4}x_{12} + 2\frac{h}{R_1^2}\dot{x}_{12}\end{cases} \tag{A.29}$$

This set of linear second-order differential equations can be solved to obtain the relative position coordinates x_{12}, y_{12} and z_{12} in the Hill reference frame, as a function of time. Consider the circular orbit of the leader satellite, and that the angular momentum is constant, $\mathbf{R_1}\cdot\mathbf{R_1} = 0$. The angular velocity of the leader equals to the frequency of revolution of the Hill frame, calculated with the mean motion Eq.(3.2),

$$\omega = n = \frac{V_1}{R_1} = \sqrt{\frac{\mu}{R_1^3}} \tag{A.30}$$

$$h = \sqrt{\mu R_1} \tag{A.31}$$

applying these substitution to the previous, yields the simplified Hill-Clohessy-Wiltshire equations:

$$\ddot{x}_{12} + 2\omega\dot{z}_{12} = 0 \tag{A.32}$$

$$\ddot{y}_{12} + \omega^2 y_{12} = 0 \tag{A.33}$$

$$\ddot{z}_{12} - 2\omega\dot{x}_{12} - 3\omega^2 z_{12} = 0 \tag{A.34}$$